Supporting Information

Supramolecular Assembly Strategy of Multinuclear Platinum(II) Complexes for Proof-of-Concept Detection and Extraction of Perfluorohexanoic Acid

Nicholas Chun-Ming Yeung, Zhen Chen, Ziyong Chen, Eric Ka-Ho Wong, Vivian Wing-Wah Yam*

Institute of Molecular Functional Materials, State Key Laboratory of Synthetic Chemistry and Department of Chemistry, The University of Hong Kong, Pokfulam Road, Hong Kong, P. R. China

*Corresponding author. E-mail: wwyam@hku.hk (V. W.-W. Y.)

Table of Contents

Physical Measurements and Instrumentation……..…3

Experimental Section…….4–8

Photophysical Studies……9

Computation Studies of Photophysical Properties…….10–19

Solution-state Supramolecular Self-assembly Studies...……20–22

Morphological Studies……...23–24

Supramolecular Self-assembly Studies Upon Addition of PFAS……...……25–30

Molecular Dynamics Simulations……...…..31–37

Extraction of PFAS from Aqueous Phase……38–50

References……...……51–52

Physical Measurements and Instrumentation

^{1}H NMR spectra were recorded on a Bruker DPX-400 (400 MHz) Fourier transform NMR spectrometer or a Bruker AVANCE 500 (500 MHz) NMR spectrometer, where the chemical shifts (in ppm) were determined with respect to tetramethylsilane (Me_4Si) as an internal reference. Matrix-assisted laser desorption ionization time-of-flight (MALDI-TOF) mass spectrometry was performed on an Applied Biosystems model MDS SCIEX 4800 Plus MALDI TOF/TOF™ Analyzer using dithranol as the matrix. UV–Visible absorption spectra were obtained by using a Varian Cary 50 UV/Vis spectrophotometer. Steady-state emission spectra were recorded using an Edinburgh Instruments FS5 spectrofluorometer. Dynamic light scattering (DLS) was performed on a Malvern Zetasizer 3000HSA with an internal HeNe laser (λ = 632.8 nm), equipped with the Varian Cary Single-Cell Peltier Thermostat. Scanning electron microscopy (SEM) experiments were performed on a Hitachi SU8010 field emission scanning electron microscope operated with an accelerating electron beam voltage of 25 kV. Transmission electron microscopy (TEM) experiments were performed using a FEI Tecnai G2 F30 field emission TEM with an accelerating electron beam voltage of 300 kV and equipped with a High-angle annular dark-field (HAADF). Atomic force microscopy (AFM) experiments were performed on a Bruker Dimension Icon AFM with standard silicon nitride cantilevers in the tapping mode. Wide-angle X-ray diffraction (WAXD) experiments were carried out using a Xenocs 3.0 HR with a 2D Hybrid Single Photon Counting detector.

Experimental Section

Materials and Reagents

Diisopropylamine (HN^iPr_2), 1,3,5-trimethylbenzene, 1,3,6,8-tetrabromopyrene, L(+)-ascorbic acid sodium salt, 2,6-dichloro-4-iodopyridine, butyric acid (C_3H_7COOH), caproic acid ($C_6H_{11}COOH$), trifluoroacetic acid (TFA) and 1-bromoperfluorohexane ($C_6F_{13}Br$), perfluorobutanesulfonic acid (PFBS) were purchased from Energy Chemical. Copper(I) iodide (CuI), copper(II) sulphate pentahydrate ($CuSO_4 \cdot 5H_2O$), silver triflate (AgOTf), perfluorobutanoic acid (PFBA) and perfluorohexanoic acid (PFHxA) were purchased from Alfa Aesar. Perfluorooctanoic acid (PFOA) and perfluorohexanesulfonic acid (PFHxS) were purchased from Beijing Minruida Technology Co., Ltd. Bis(triphenylphosphine)palladium(II) chloride ($[PdCl_2(PPh_3)_2]$)[1], tetrakis(triphenylphosphine)palladium(0) ($[Pd(PPh_3)_4]$),[2] *cis*-dichlorobis(dimethyl sulfoxide)platinum(II) ($[Pt(DMSO)_2Cl_2]$),[3] 1-azidododecane ($C_{12}H_{25}N_3$)[4] and the 2,6-bis(1,2,3-triazol-4-yl)-pyridine (btp) moieties were synthesized as reported in the literature with modified procedures.[5-7] All amines were distilled over sodium hydroxide before use. Other solvents for synthesis were used as received. Deionized water was produced by a Milli-Q apparatus (Millipore).

Synthesis

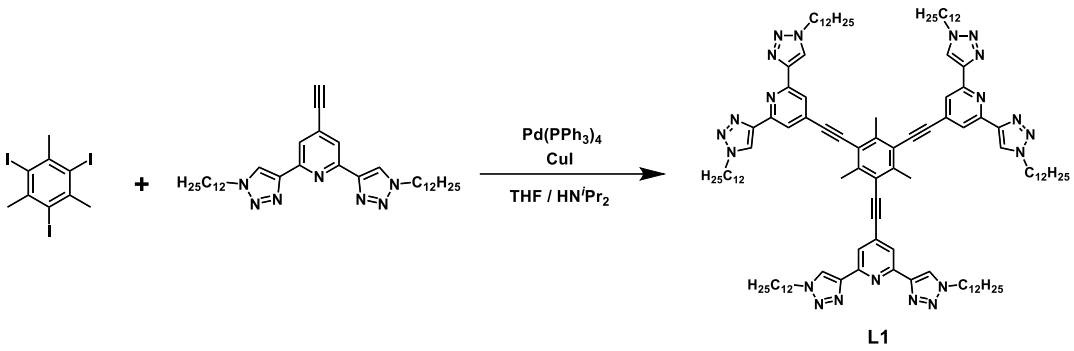

Ligand L1. To a degassed THF/HN^iPr_2 solution (40 mL, 3/1 v/v) of 1,3,5-triiodo-2,4,6-trimethylbenzene (0.600 g, 1.21 mmol, 1 eqv.) and 2,6-bis(1-dodecyl-1*H*-1,2,3-triazol-4-yl)-4-ethynylpyridine (2.50 g, 4.40 mmol, 3.6 eqv.) were added [$Pd(PPh_3)_4$] (0.173 g, 0.15 mmol, 0.12 eqv.) and CuI (30 mg, 0.15 mmol, 0.12 eqv.). The reaction mixture was refluxed for 48 hours under nitrogen atmosphere. The resulting mixture was then extracted with $CHCl_3$ and deionized water for three times, and the combined organic extract was dried over anhydrous $MgSO_4$. After concentration, the crude product was subjected to column chromatography (SiO_2, $CHCl_3$). The collected fraction was evaporated to dryness to yield a yellow solid. Recrystallization by layering of MeOH to a $CHCl_3$ solution of the isolated solid afforded **L1** as a white solid. Yield: 74%. ^{1}H NMR (500 MHz, $CDCl_3$, 298 K, relative to Me_4Si, δ/ ppm): δ 8.23 (s, 6H, triazo), 8.21 (s, 6H, py), 4.47 (t, J = 7.00 Hz, 12H, triazo–CH_2–), 2.84 (s, 9H, Ph–CH_3). 1.99 (t, J = 7.00 Hz, 12H, triazo–CH_2–CH_2–), 1.25 (m, 24H, –CH_2–), 1.24 (m, 84H, –CH_2–), 0.87 (t, J = 7.00 Hz, 18H, –CH_3). Positive ESI-MS: calcd. for $C_{114}H_{171}N_{21}Na_2$ $[M+2Na]^{2+}$: m/z = 940.6921; found: 940.6875.

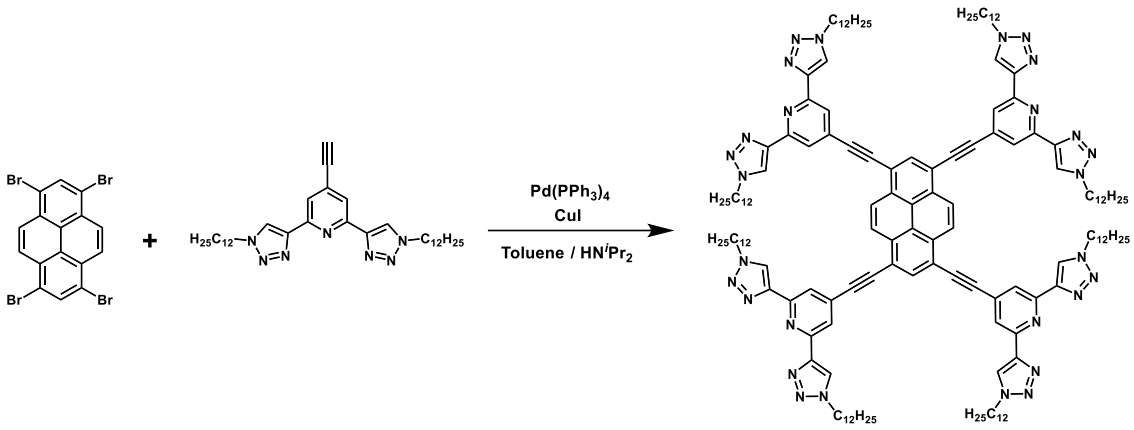

Ligand L2. To a degassed toluene/HN^iPr_2 solution (30 mL, 1/1 v/v) of 1,3,6,8-tetrabromopyrene (0.140 g, 0.268 mmol, 1 eqv.) and 2,6-bis(1-dodecyl-1*H*-1,2,3-triazol-4-yl)-4-ethynylpyridine (0.740 g, 1.49 mmol, 4.8 eqv.) were added [$Pd(PPh_3)_4$] (37 mg, 0.03 mmol, 0.12 eqv.) and CuI (6 mg, 0.03 mmol, 0.12 eqv.). The reaction mixture was refluxed for 48 hours under nitrogen atmosphere. Then, the resulting mixture was extracted with $CHCl_3$ and deionized water for three times, and the combined organic extract was dried over anhydrous $MgSO_4$. After concentration, the crude product was subjected to column chromatography (SiO_2, $CHCl_3$). The collected fraction was evaporated to dryness to yield an orange solid. Recrystallization by layering of MeOH to a $CHCl_3$ solution of the isolated solid afforded **L2** as an orange solid. Yield: 17%. ^{1}H NMR (500 MHz, $CDCl_3$, 298 K, relative to Me_4Si, δ/ ppm): δ 8.83 (s, 4H, pyrene), 8.56 (s, 2H, pyrene), 8.35 (s, 8H, triazo), 8.25 (s, 8H, py), 4.45 (t, J = 7.00 Hz, 16H, triazo–CH_2–), 2.00 (quintet, J = 7.00 Hz, 16H, –CH_2–). 1.38 (m, 16H, –CH_2–), 1.26 (m, 56H, –CH_2–), 0.87 (t, J = 7.00 Hz, 12H, –CH_3). MALDI-TOF MS: calcd. for $C_{156}H_{222}N_{28}$ $[M]^+$: m/z = 2489.834; found: 2490.105.

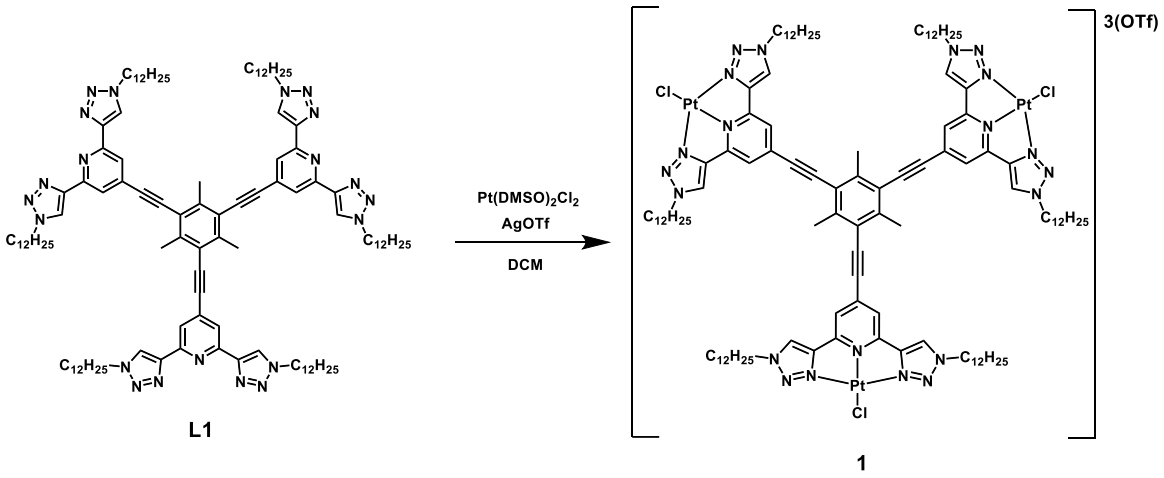

Complex 1. To an acetone solution (100 mL) of [Pt(DMSO)Cl_2] (77 mg, 0.182 mmol, 3.2 eqv.) was added an AgOTf (47 mg, 0.182 mmol, 3.2 eqv.) in acetone (100 mL) dropwise. The mixture was stirred for 3 hours at room temperature under nitrogen atmosphere. After filtration, the filtrate was collected and was concentrated to 5 mL. Then, the concentrated solution was transferred to a dichloromethane solution (30 mL) of **L1** (0.100 g, 0.0568 mmol, 1 eqv.). After stirring overnight at room temperature, the reaction mixture was concentration under reduced pressure and MeOH was added to precipitate the product as a yellow solid. The yellow solid was collected through filtration and was washed with MeOH and acetonitrile. Recrystallization by layering of MeOH to a $CHCl_3$ solution of the crude afforded **1** as a yellow solid. Yield: 58%. ^{1}H NMR (500 MHz, $CDCl_3$, 298 K, relative to Me_4Si, δ/ ppm): δ 9.10 (s, 6H, triazo), 8.16 (s, 6H, py), 4.67 (m, 12H, triazo–CH_2–), 2.86 (s, 9H, Ph–CH_3). 2.09 (m, 12H, triazo–CH_2–CH_2–), 1.39–1.26 (m, 108H, –CH_2–), 0.87 (s, 18H, J = 5.00 Hz, –CH_3). MALDI-TOF MS: calcd. for $C_{116}H_{171}Cl_3F_6N_{21}O_6Pt_3S_2$ $[M–OTf]^+$: m/z = 2825.107; found: 2825.112.

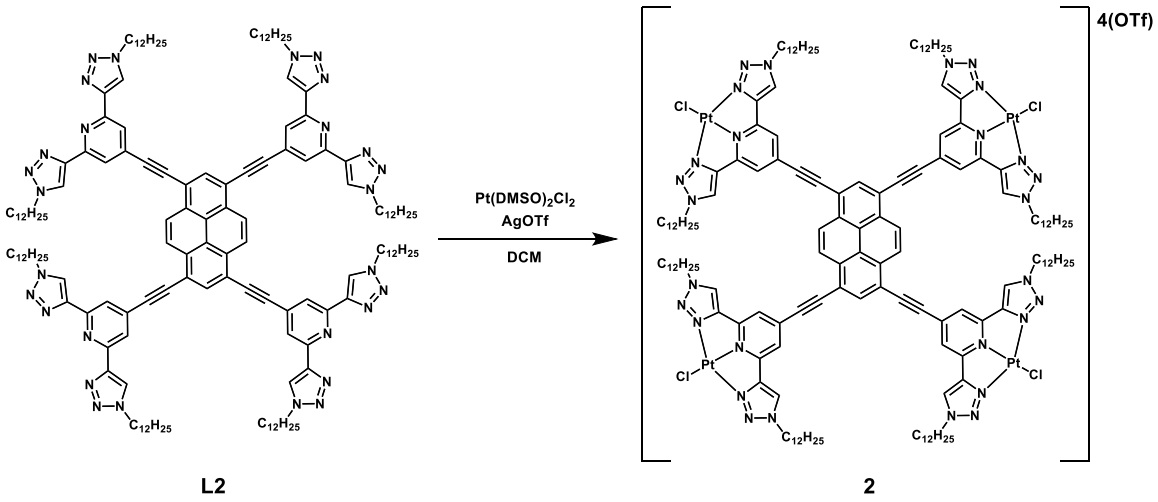

Complex 2. To an acetone solution (100 mL) of $[Pt(DMSO)_2Cl_2]$ (91 mg, 0.216 mmol, 4.9 eqv.) was added AgOTf (54 mg, 0.216 mmol, 4.9 eqv.) in acetone (100 mL) dropwise. The mixture was stirred for 3 hours at room temperature under nitrogen atmosphere. After filtration, the filtrate was collected and concentrated to 5 mL. Then, the concentrated solution was transferred to a dichloromethane solution (30 mL) of **L2** (0.11 g, 0.0462 mmol, 1 eqv.). After stirring overnight at room temperature, the reaction mixture was concentration under reduced pressure and MeOH was added to precipitate the product as a red solid. The red solid was collected through filtration and was washed with MeOH and acetonitrile. Recrystallization by layering of MeOH to a DCM solution of the crude afforded **2** as a dark red solid. Yield: 68%. MALDI-TOF MS: calcd. for $C_{159}H_{222}Cl_4F_9N_{28}O_9Pt_4S_3$ $[M–OTf]^+$: *m/z* = 3858.414; found: *m/z* = 3858.671.

Photophysical Studies

Table S1 Photophysical data of **1** and **2** in $CHCl_3$ at 298 K.

Complex	λ_{abs} / nm (ε / mol^{-1} dm^3 cm^{-1})	λ_{em} / nm (τ_0 / μs)
1	347 (43700), 397 (95000), 412 (110300)	549, 594 (0.3)
2	327 (47100), 422 (58300), 477 (40300), 511 (40800), 548 (30600)	564, 607 (0.2)

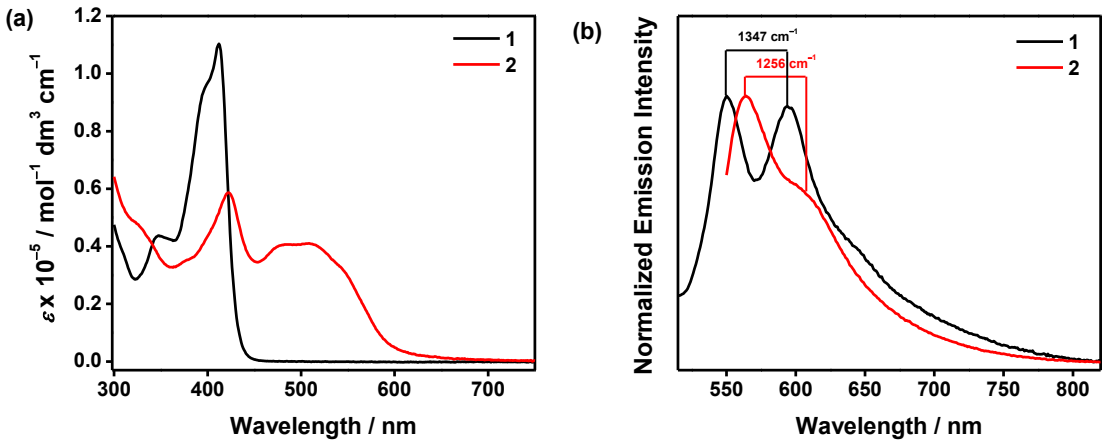

Figure S1 (a) UV–Vis absorption and (b) emission spectra of **1** and **2** in $CHCl_3$ at 298 K.

Computational Studies of Photophysical Properties

Quantum Chemical Calculations

All DFT and TDDFT calculations were performed using Gaussian 16 (revision C.01) package.[8] The optimized ground-state (S_0) geometries of solvent molecules (*n*-hexane, $CHCl_3$, $C_5F_{11}COOH$, $C_5H_{11}COOH$ and $C_6F_{13}Br$), OTf^- anion, and model complex cations **1′**, **2′** and **3** were computed at PBE0-D3BJ level.[9] The Stuttgart effective core potentials (SDD) and the associated basis set were used to describe platinum,[10] whereas the 6-31G(d,p) basis set was used for all other atoms. The bulk solvent effect in the *n*-hexane environment was simulated using the polarizable continuum model (PCM),[11] considering that the dielectric constants of *n*-hexane and $CHCl_3$ are comparable. Restrained electrostatic potential (RESP) atomic charges[12] were computed using Multiwfn (version 3.8dev) package[13] for atomistic molecular dynamics (MD) simulations. Cartesian coordinates of the optimized S_0 state structures of **1′**, **2′** and **3** are provided in Table S3, Table S4 and Table S8. On the basis of the optimized S_0 geometries, TDDFT calculations at the same level associated with PCM(*n*-hexane) were performed to compute the singlet–singlet transitions.

DFT and TDDFT calculations

To gain deeper insights into the nature of absorption origins, density functional theory (DFT) and time-dependent DFT (TDDFT) calculations have been performed on model complex cations **1′** and **2′** where all the $–C_{12}H_{25}$ chains are simplified to $–CH_3$ group (Table S2 and Figure S2–Figure S5). For **1′**, the low-energy bands at 350–450 nm are assigned as the metal-to-ligand charge transfer (^{1}MLCT) [dπ(Pt) → π^*(btp)] (S_1 and S_2 states) and intraligand (^{1}IL) [π(mesitylene) → π^*(btp)] (S_{19} and S_{20} states) transitions (Figure S4). The high-energy absorption bands can be assigned as the mixture of metal-perturbed intraligand charge-transfer (^{1}ILCT) [π(C≡C) → π^*(btp)] and [π(C≡C) → π^*(mesitylene)] (S_{73} and S_{74} states) transitions. For **2′**, our computational results suggest that the lowest-energy absorption band arise from the HOMO→LUMO excitation. The HOMO of **2′** is mainly

localized on the pyrene moiety while the LUMO distributes on both the pyrene and btp moieties (Figure S3). Thus, the lowest-energy absorption band can be assigned as the ^{1}IL [$\pi \rightarrow \pi^*$(pyrene)] transitions with minor contributions from the ^{1}ILCT [π(pyrene) $\rightarrow$ π^*(btp)] character, as reflected from hole-electron analysis on the S_1 state (Figure S5). The low-energy absorption bands at around 460 nm mainly arise from the HOMO–1→LUMO, HOMO–2→LUMO, HOMO→LUMO+1, and HOMO→LUMO+2 excitations, which can be assigned as the mixing of ^{1}MLCT [dπ(Pt) $\rightarrow$ π^*(pyrene)] and ^{1}ILCT [π(pyrene) $\rightarrow$ π^*(btp)] (S_2 and S_3 states) transitions. The high-energy absorption bands at around 380 nm (S_{26} state) and 320 nm (S_{77} state) are mainly dominated by the ^{1}IL [$\pi \rightarrow \pi^*$(pyrene)] transitions.

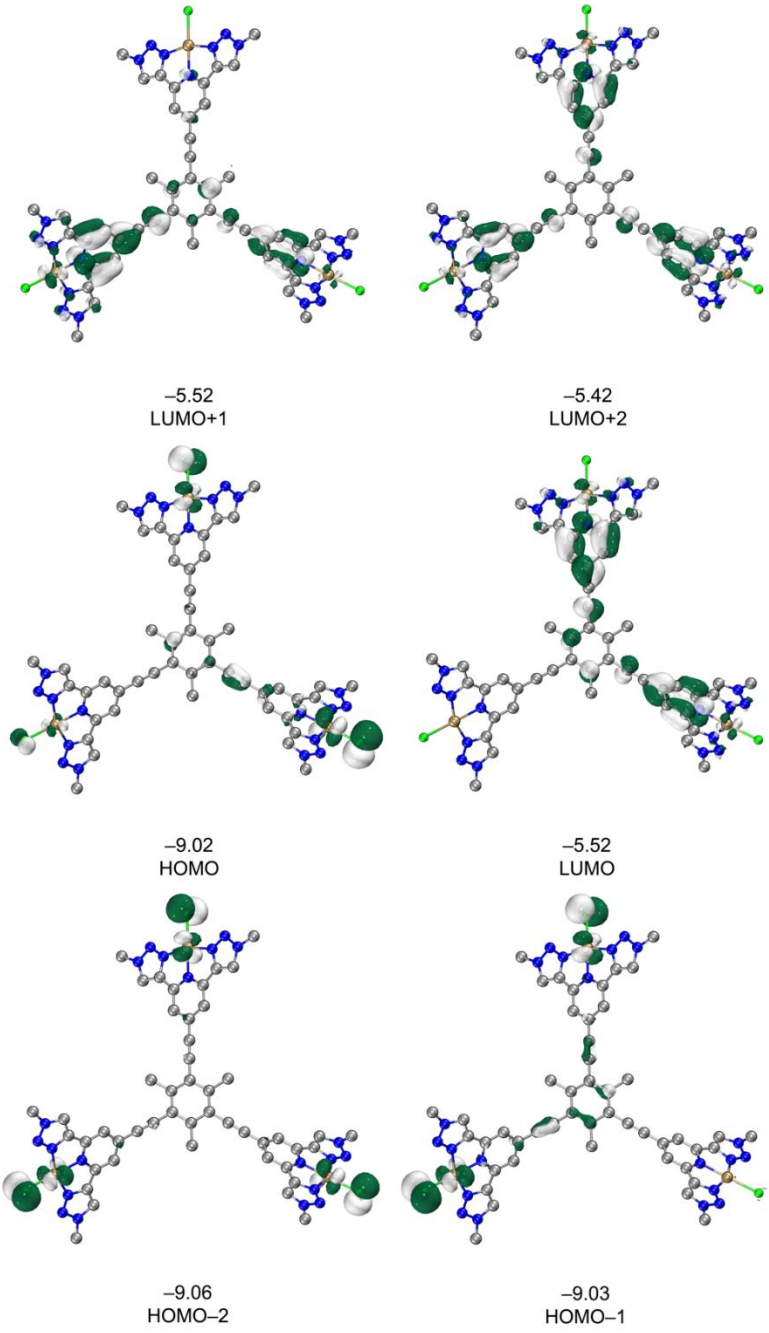

Figure S2 Spatial plots (isovalue = 0.03) of selected frontier molecular orbitals of **1′** obtained from the PBE0/PCM (*n*-hexane) calculation. MO energies (eV) are provided.

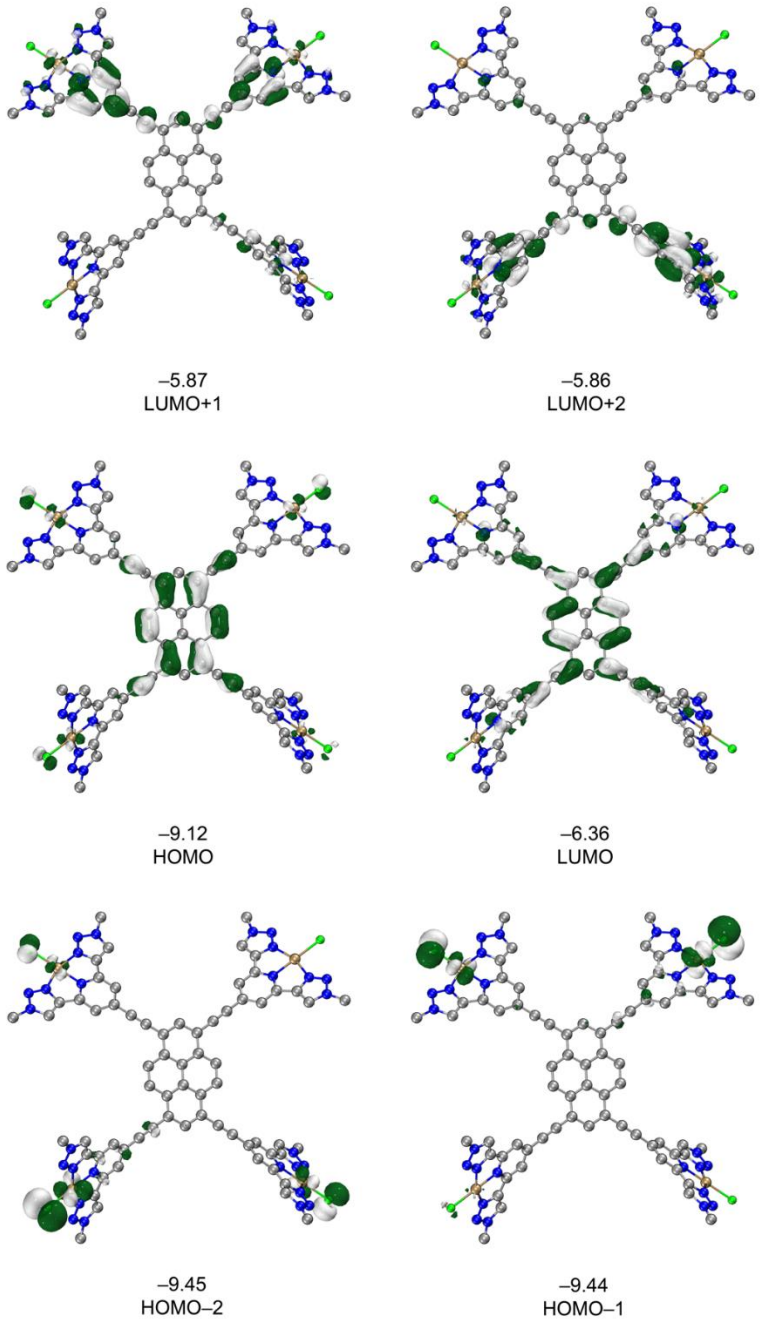

Figure S3 Spatial plots (isovalue = 0.03) of selected frontier molecular orbitals of **2′** obtained from the PBE0/PCM (*n*-hexane) calculation. MO energies (eV) are provided.

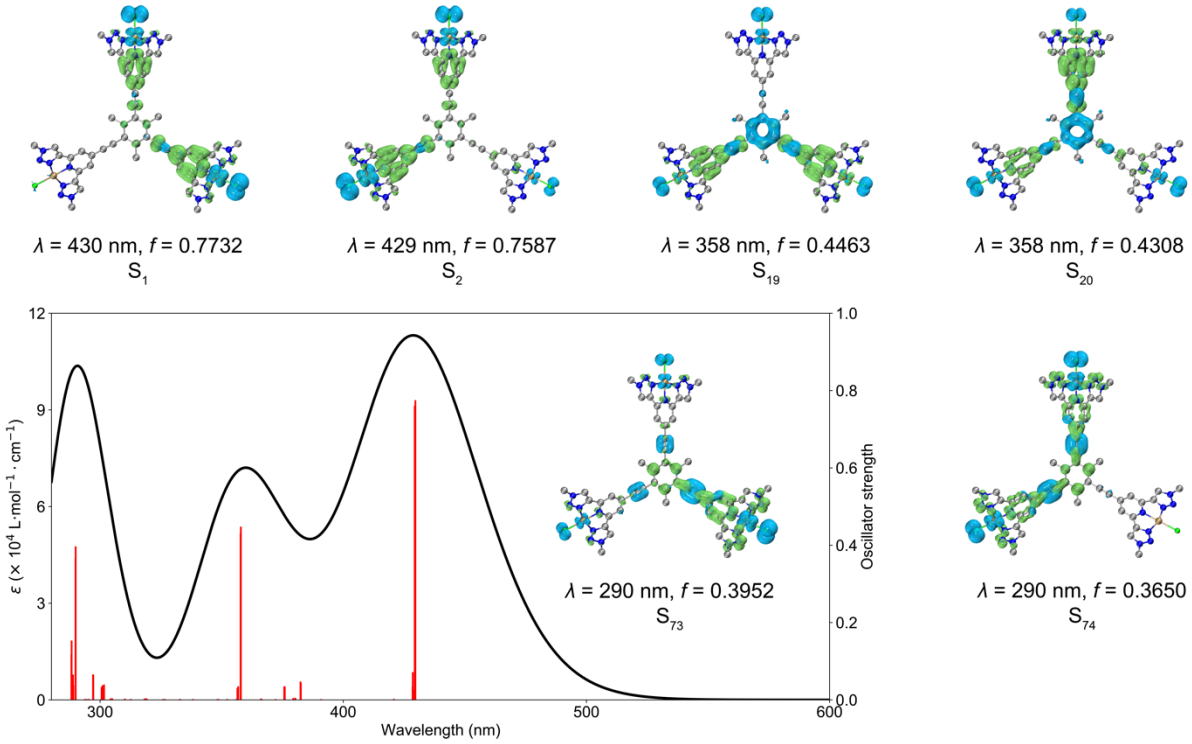

Figure S4 Simulated absorption spectrum of **1′**. The vertical lines refer to the unbroadened oscillator strengths of the singlet–singlet transitions. Distributions (isovalue = 0.001) of the hole (blue) and electron (lime) for selected singlet excited states are computed at the optimized S_0 geometry.

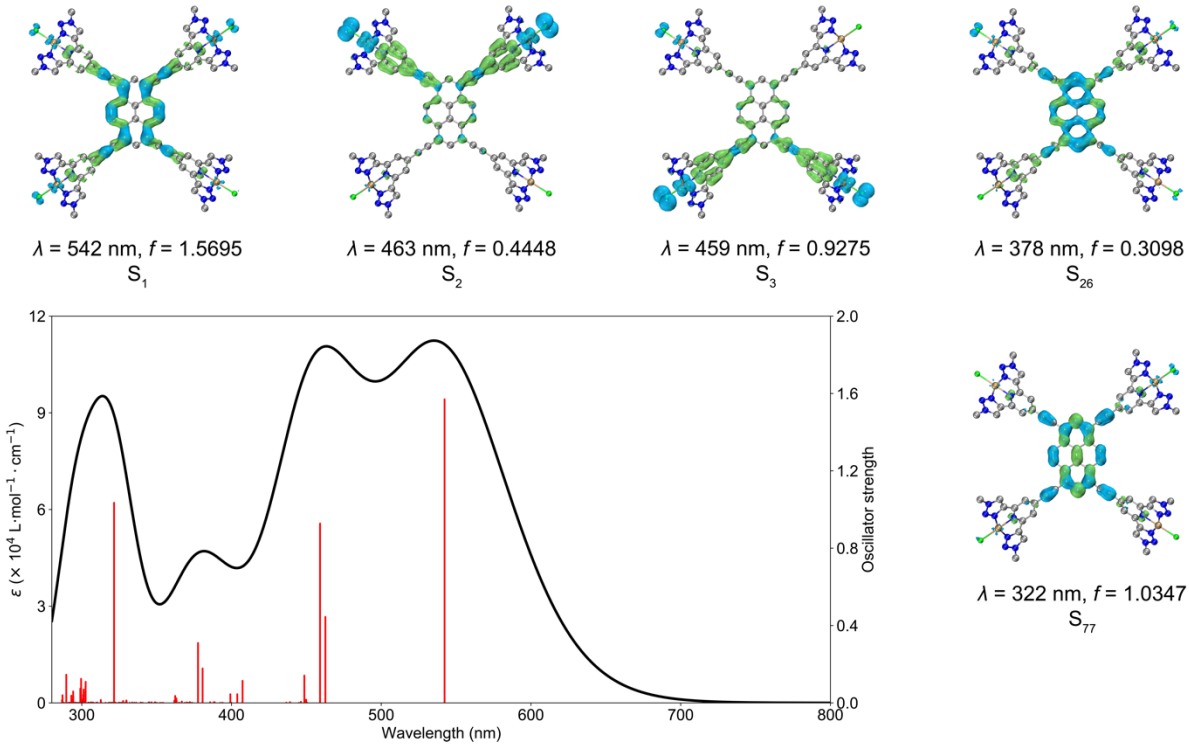

Figure S5 Simulated absorption spectrum of **2′**. The vertical lines refer to the unbroadened oscillator strengths of the singlet–singlet transitions. Distributions (isovalue = 0.001) of the hole (blue) and electron (lime) for selected singlet excited states are computed at the optimized S_0 geometry.

Table S2 The singlet excited states with the vertical excitation wavelength > 400 nm computed by TDDFT/PCM (*n*-hexane) at the optimized S_0 geometry

Complex	S_n	Excitation (Coefficient)[b]	λ[c] / nm	*f*[d]
1′	S_1	H→L+2 (0.35) H–2→L (–0.33)	430	0.773
	S_2	H–2→L+1 (0.35) H–1→L+2 (0.34)	429	0.759
	S_3	H–3→L (0.45) H–3→L+1 (0.37) H–3→L+2 (–0.37)	429	0.024
	S_4	H–4→L (0.50) H–4→L+2 (0.34)	429	0.070
	S_5	H–5→L+1 (0.55) H–5→L+2 (0.35)	429	0.034
	S_6	H–1→L+1 (0.38) H→L (–0.36) H–2→L+2 (0.33)	421	0.001
2′	S_1	H→L (0.69)	542	1.569
	S_2	H–1→L (0.52) H→L+1 (0.41)	463	0.445
	S_3	H–2→L (0.53) H→L+2 (–0.37)	459	0.928
	S_4	H–5→L (0.54)	451	0.000
	S_5	H–3→L (0.50)	450	0.016
	S_6	H–6→L (0.49)	450	0.002
	S_7	H–7→L (0.53) H–7→L+1 (0.36)	449	0.000
	S_8	H→L+2 (0.42) H→L+1 (0.38) H–1→L (–0.35)	449	0.141
	S_9	H→L+1 (0.37) H→L+2 (–0.35) H–3→L (–0.33)	446	0.006
	S_{10}	H–8→L (0.49) H–8→L+2 (0.39)	445	0.000
	S_{11}	H→L+3 (0.67)	439	0.004
	S_{12}	H–4→L (0.64)	437	0.001
	S_{13}	H–3→L+2 (0.34) H–2→L+2 (0.33)	407	0.114
	S_{14}	H–1→L+1 (0.44)	404	0.045

[a]The orbitals involved in the excitation (H = HOMO and L = LUMO). [b]The coefficients in the configuration interaction (CI) expansion that are less than 0.3 are not listed.

Table S3 Cartesian coordinates of the optimized S_0 structure of **1′**

1	C	1.315884	–0.636786	–0.092434	**58**	H	2.796366	11.551869	3.607794
2	C	0.197464	–1.497783	–0.090685	**59**	C	–4.941502	9.725042	–3.755222
3	C	–1.086180	–0.927725	–0.070788	**60**	H	–4.609670	9.487419	–4.766612
4	C	–1.273420	0.471293	–0.056060	**61**	H	–5.890859	9.233970	–3.539776
5	C	–0.137512	1.298443	–0.062387	**62**	H	–5.046772	10.802555	–3.642636
6	C	1.167494	0.761124	–0.078407	**63**	C	–6.251034	–9.171746	–3.724889
7	C	–2.239322	–1.760214	–0.060291	**64**	H	–6.157149	–8.782592	–4.739609
8	C	–3.250575	–2.434852	–0.046135	**65**	H	–5.386193	–9.786162	–3.471579
9	C	–4.425087	–3.227386	–0.025225	**66**	H	–7.163822	–9.757502	–3.633749
10	C	–5.498084	–2.882898	0.818314	**67**	C	–10.522715	–2.671133	3.832980
11	C	–4.525137	–4.366018	–0.847416	**68**	H	–10.647000	–1.595948	3.701386
12	C	–6.632065	–3.678785	0.817474	**69**	H	–11.467970	–3.180853	3.656145
13	H	–5.431230	–2.013830	1.462070	**70**	H	–10.162254	–2.890368	4.839284
14	C	–5.689374	–5.116277	–0.812083	**71**	C	2.615969	–1.213362	–0.100746
15	H	–3.706307	–4.643736	–1.500687	**72**	C	3.721636	–1.718684	–0.101007
16	C	–7.850273	–3.534129	1.603800	**73**	C	5.019589	–2.286411	–0.092938
17	N	–6.698785	–4.757672	0.009063	**74**	C	6.034178	–1.736221	–0.898214
18	C	–6.027918	–6.311110	–1.574134	**75**	C	5.306788	–3.391596	0.729499
19	C	–8.339415	–2.685480	2.567938	**76**	C	7.300203	–2.297157	–0.857422
20	N	–8.838741	–4.468259	1.392542	**77**	H	5.823830	–0.884286	–1.532825
21	Pt	–8.349355	–5.856123	0.020556	**78**	C	6.594093	–3.903714	0.734795
22	C	–5.434931	–7.107367	–2.524327	**79**	H	4.534847	–3.816995	1.359603
23	N	–7.267037	–6.863751	–1.343884	**80**	C	8.497441	–1.905141	–1.590600
24	H	–7.928451	–1.815199	3.056145	**81**	N	7.544844	–3.348908	–0.046894
25	N	–9.568810	–3.168154	2.854488	**82**	C	7.131769	–5.012311	1.512276
26	N	–9.866381	–4.245095	2.143640	**83**	C	8.850147	–0.965296	–2.529962
27	Cl	–10.257161	–7.129290	0.036927	**84**	N	9.642810	–2.623091	–1.332577
28	H	–4.475033	–7.066847	–3.014482	**85**	Pt	9.383710	–4.086705	0.023705
29	N	–6.351396	–8.065338	–2.786351	**86**	C	6.666329	–5.926959	2.426328
30	N	–7.455797	–7.915824	–2.070567	**87**	N	8.470175	–5.290583	1.353750
31	C	–0.289621	2.713131	–0.048204	**88**	H	8.294443	–0.190713	–3.035722
32	C	–0.399155	3.923536	–0.038476	**89**	N	10.163345	–1.188562	–2.758325
33	C	–0.547857	5.332706	–0.027662	**90**	N	10.638300	–2.190360	–2.033643
34	C	–1.523121	5.945287	–0.837690	**91**	Cl	11.516374	–4.922571	0.117152
35	C	0.273367	6.128095	0.793391	**92**	H	5.691955	–6.102219	2.854128
36	C	–1.648246	7.325060	–0.809104	**93**	N	7.747750	–6.671866	2.744218
37	H	–2.155824	5.341427	–1.477401	**94**	N	8.835386	–6.284487	2.094991
38	C	0.088336	7.500957	0.792848	**95**	C	7.828669	–7.775414	3.687750
39	H	1.030760	5.671039	1.419249	**96**	H	7.679235	–7.402809	4.702173
40	C	–2.550484	8.179466	–1.571645	**97**	H	7.068944	–8.517030	3.439960
41	N	–0.853124	8.056331	0.000788	**98**	H	8.821448	–8.211561	3.594547
42	C	0.790869	8.514098	1.567984	**99**	C	–2.657624	1.036583	–0.032290
43	C	–3.524113	8.030038	–2.530590	**100**	H	–3.228279	0.692460	–0.901005
44	N	–2.458153	9.533755	–1.343468	**101**	H	–3.195121	0.692447	0.857580
45	Pt	–1.064265	10.027058	0.018638	**102**	H	–2.644523	2.126870	–0.028605
46	C	1.787562	8.552627	2.512661	**103**	C	0.397520	–2.979960	–0.103620
47	N	0.412580	9.822171	1.369880	**104**	H	0.990945	–3.281856	–0.972807
48	H	–3.934934	7.166015	–3.028651	**105**	H	0.951356	–3.298691	0.785850
49	N	–3.937004	9.288994	–2.797790	**106**	H	–0.554525	–3.510503	–0.126608
50	N	–3.290559	10.194004	–2.078871	**107**	C	2.347511	1.680143	–0.078048
51	Cl	–1.293787	12.308149	0.024777	**108**	H	2.323828	2.336230	–0.954539
52	H	2.378616	7.782310	2.982645	**109**	H	2.328691	2.326069	0.806152
53	N	1.929326	9.864159	2.804904	**110**	H	3.286064	1.125692	–0.081420
54	N	1.096663	10.627922	2.113618	**111**	C	11.051754	–0.480248	–3.666092
55	C	2.827680	10.476267	3.770857	**112**	H	10.710662	–0.616976	–4.692768
56	H	2.491761	10.242868	4.782258	**113**	H	11.066956	0.579152	–3.408076
57	H	3.838083	10.100795	3.609212	**114**	H	12.045311	–0.907474	–3.544452

Table S4 Cartesian coordinates of the optimized S_0 structure of **2′**

1	C	0.104226	–3.524866	0.089689	**76**	C	5.768323	7.017593	–0.575984
2	C	1.303370	–2.809597	0.082710	**77**	H	3.817810	6.488693	–1.316221
3	C	1.285281	–1.390356	0.103157	**78**	C	6.677924	5.642964	1.126818
4	C	0.032111	–0.718758	0.100873	**79**	H	5.488888	3.967591	1.769494
5	C	–1.184238	–1.453574	0.109113	**80**	C	6.118915	8.189113	–1.367833
6	C	–1.130111	–2.871771	0.115602	**81**	N	6.751718	6.702265	0.293220
7	C	2.484775	–0.620810	0.133754	**82**	C	7.869935	5.544190	1.957785
8	C	–0.007624	0.707472	0.087070	**83**	C	5.552750	8.941608	–2.370096
9	C	1.207875	1.443401	0.114538	**84**	N	7.343398	8.764076	–1.117248
10	C	2.446209	0.739982	0.145839	**85**	Pt	8.376293	7.839329	0.338845
11	C	1.153629	2.861850	0.095864	**86**	C	8.339829	4.730915	2.961578
12	C	–0.080075	3.512899	0.036770	**87**	N	8.841038	6.499645	1.767370
13	C	–1.278877	2.797288	0.010449	**88**	H	4.606109	8.876294	–2.882824
14	C	–1.260550	1.378179	0.046924	**89**	N	6.470421	9.895003	–2.640209
15	C	–2.460829	0.609926	0.059369	**90**	N	7.550276	9.785839	–1.880954
16	C	–2.422920	–0.750173	0.097221	**91**	Cl	10.262452	9.142597	0.381188
17	H	–3.340086	–1.329614	0.112461	**92**	H	7.926534	3.864370	3.454240
18	H	–3.412138	1.133763	0.047699	**93**	N	9.540073	5.255353	3.291276
19	H	3.436535	–1.143872	0.148489	**94**	N	9.840463	6.323077	2.567614
20	H	0.129961	–4.608965	0.080349	**95**	C	–2.504092	3.510807	–0.050350
21	H	3.363335	1.319280	0.167839	**96**	C	–3.542427	4.141158	–0.105049
22	H	–0.107186	4.596447	0.015237	**97**	C	–4.743364	4.892749	–0.164465
23	C	2.530115	–3.524071	0.041521	**98**	C	–4.918967	6.003675	0.682208
24	C	3.565983	–4.158493	–0.004844	**99**	C	–5.763930	4.539056	–1.066783
25	C	4.763266	–4.916074	–0.089006	**100**	C	–6.099338	6.724768	0.605544
26	C	5.662627	–4.700039	–1.149548	**101**	H	–4.147132	6.283573	1.389035
27	C	5.046870	–5.895363	0.879068	**102**	C	–6.915010	5.310810	–1.110134
28	C	6.812431	–5.473183	–1.220063	**103**	H	–5.644388	3.690178	–1.730746
29	H	5.441671	–3.943852	–1.893961	**104**	C	–6.506285	7.893231	1.374342
30	C	6.209404	–6.639248	0.757074	**105**	N	–7.050633	6.368567	–0.283279
31	H	4.368580	–6.051622	1.709004	**106**	C	–8.078606	5.168000	–1.974551
32	C	7.883596	–5.443097	–2.210700	**107**	C	–5.987933	8.675872	2.378316
33	N	7.046588	–6.413295	–0.278119	**108**	N	–7.738866	8.429557	1.080833
34	C	6.707819	–7.700929	1.622124	**109**	Pt	–8.707970	7.453592	–0.386620
35	C	8.190819	–4.751897	–3.360448	**110**	C	–8.487913	4.333958	–2.987444
36	N	8.922313	–6.326837	–2.023211	**111**	N	–9.087890	6.089281	–1.818644
37	Pt	8.709367	–7.487956	–0.396616	**112**	H	–5.054973	8.643543	2.920453
38	C	6.295078	–8.370706	2.750745	**113**	N	–6.935859	9.612109	2.603511
39	N	7.909774	–8.271636	1.271367	**114**	N	–7.990908	9.461296	1.816878
40	H	7.684919	–3.967615	–3.901693	**115**	Cl	–10.624627	8.709081	–0.492256
41	N	9.372662	–5.266054	–3.763456	**116**	H	–8.031487	3.473093	–3.449177
42	N	9.810744	–6.218477	–2.955128	**117**	N	–9.696647	4.811564	–3.354991
43	Cl	10.642933	–8.715478	–0.518196	**118**	N	–10.055285	5.873771	–2.648756
44	H	5.423299	–8.290402	3.379706	**119**	C	–10.604113	4.293577	–4.367404
45	N	7.267700	–9.278542	2.983386	**120**	H	–10.088223	3.513668	–4.925759
46	N	8.241933	–9.215887	2.088643	**121**	H	–11.490518	3.884572	–3.880588
47	C	–2.319744	–3.644717	0.146319	**122**	H	–10.887941	5.105789	–5.036289
48	C	–3.330285	–4.320900	0.168334	**123**	C	–6.895123	10.729680	3.533884
49	C	–4.503562	–5.115987	0.208714	**124**	H	–6.470469	10.393136	4.479165
50	C	–5.548356	–4.790682	1.094253	**125**	H	–6.291587	11.536076	3.113462
51	C	–4.629772	–6.234715	–0.636673	**126**	H	–7.917462	11.071523	3.684713
52	C	–6.673743	–5.598860	1.123430	**127**	C	–10.440079	–4.678293	4.317431
53	H	–5.460855	–3.935864	1.755076	**128**	H	–10.728667	–5.503231	4.968412
54	C	–5.790011	–6.989926	–0.578268	**129**	H	–9.943450	–3.900916	4.896959
55	H	–3.836640	–6.492345	–1.328106	**130**	H	–11.321253	–4.271528	3.819503
56	C	–7.855585	–5.487240	1.965934	**131**	C	–6.448552	–10.999113	–3.539014
57	N	–6.764967	–6.660271	0.294948	**132**	H	–5.493467	–10.948567	–4.059973
58	C	–6.154616	–8.166084	–1.356382	**133**	H	–6.529134	–11.942403	–2.998030
59	C	–8.304131	–4.665003	2.971167	**134**	H	–7.270701	–10.906822	–4.249077
60	N	–8.839311	–6.432224	1.790161	**135**	C	10.142510	–4.938738	–4.952743

61	Pt	–8.398069	–7.783991	0.362660	**136**	H	9.954008	–5.686637	–5.724779
62	C	–5.594397	–8.941204	–2.344691	**137**	H	9.841130	–3.952485	–5.302627
63	N	–7.381134	–8.730038	–1.091084	**138**	H	11.199034	–4.937350	–4.688526
64	H	–7.874169	–3.799536	3.448912	**139**	C	7.357379	–10.245371	4.067892
65	N	–9.506793	–5.172388	3.316776	**140**	H	8.094812	–9.908371	4.797879
66	N	–9.827538	–6.240770	2.601663	**141**	H	6.377283	–10.329309	4.535891
67	Cl	–10.292535	–9.074409	0.426262	**142**	H	7.657468	–11.206005	3.651237
68	H	–4.648230	–8.890622	–2.860457	**143**	C	10.500124	4.764078	4.266684
69	N	–6.514335	–9.899443	–2.588389	**144**	H	9.977727	4.111373	4.963714
70	N	–7.592195	–9.769528	–1.829417	**145**	H	11.288969	4.211883	3.752720
71	C	2.340215	3.638714	0.145373	**146**	H	10.925045	5.616599	4.794628
72	C	3.346947	4.319970	0.181682	**147**	C	6.419973	10.946685	–3.644648
73	C	4.509903	5.129962	0.222971	**148**	H	5.416386	10.976593	–4.066230
74	C	4.618003	6.247219	–0.626992	**149**	H	6.655049	11.898709	–3.169535
75	C	5.561601	4.821969	1.106755	**150**	H	7.150364	10.731757	–4.425528

Solution-state Supramolecular Self-assembly Studies

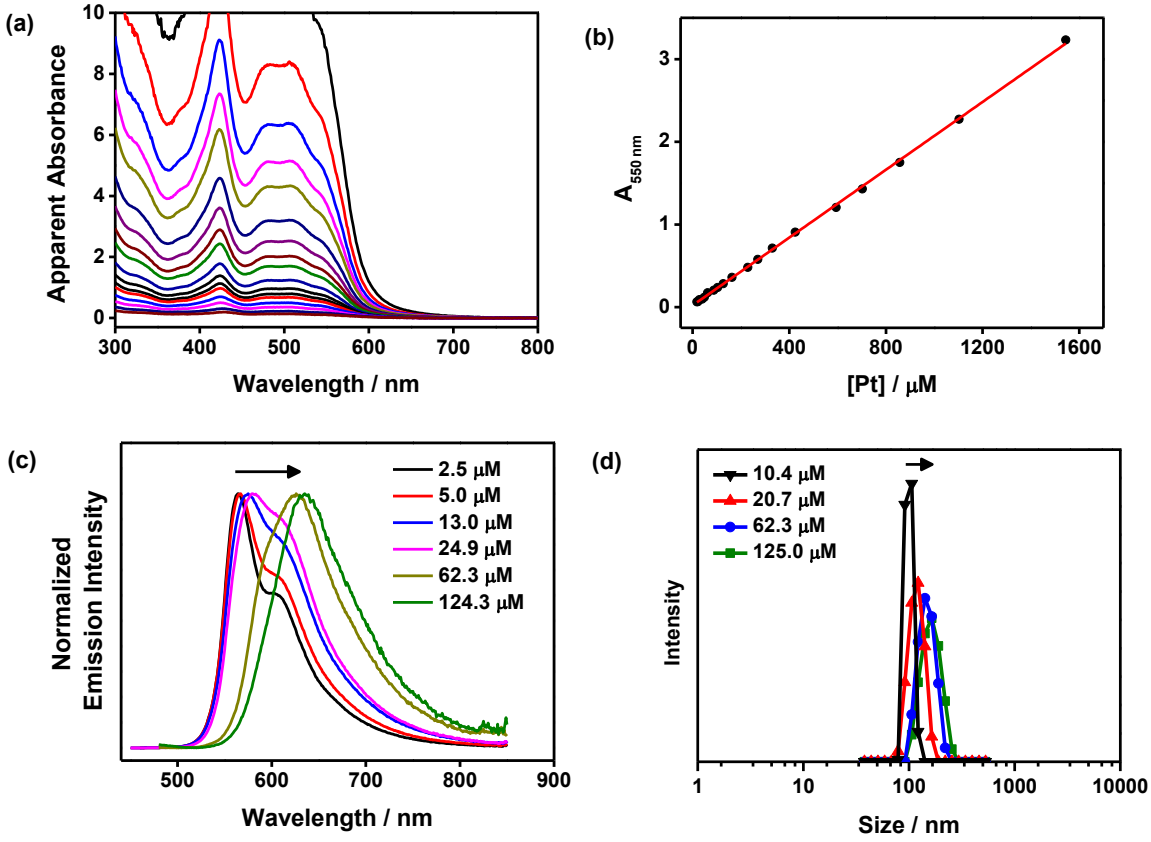

Figure S6 (a) Concentration-dependent UV−vis absorption spectra of **2** in $CHCl_3$ with concentration ranges from 4.52 to 386 μM. The apparent absorbance values have been obtained by correcting to 1-cm path length equivalence. (b) A plot of absorbance monitored at 580 nm against concentration.(c) Concentration-dependent normalized emission spectra and (d) DLS traces of **2** in $CHCl_3$. The excitation wavelength is 430 nm.

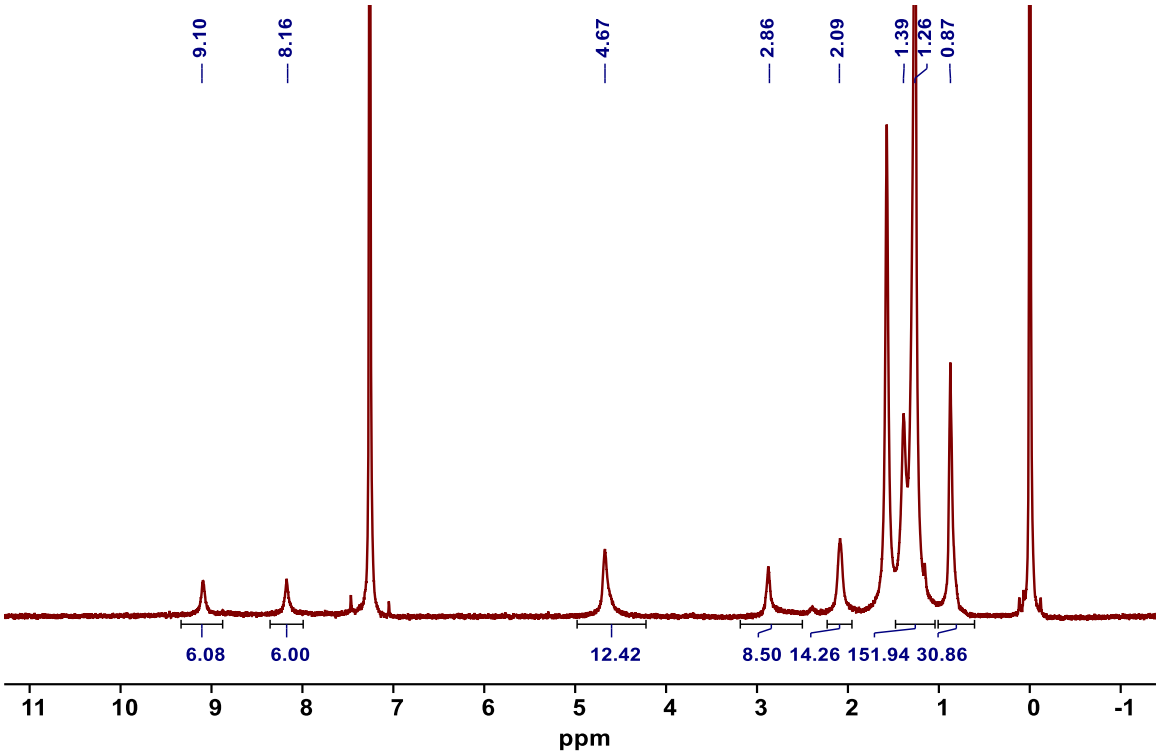

Figure S7 ^{1}H NMR spectrum of **1** in $CDCl_3$ at 298 K.

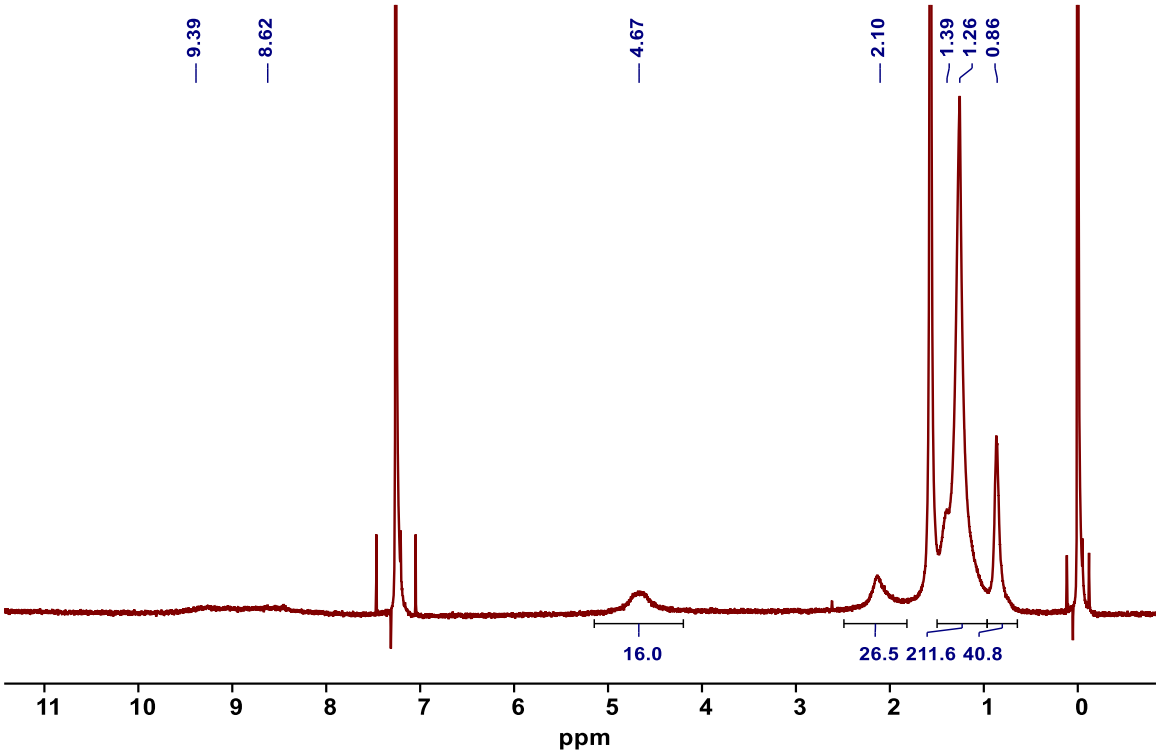

Figure S8 ^{1}H NMR spectrum of **2** in $CDCl_3$ at 298 K.

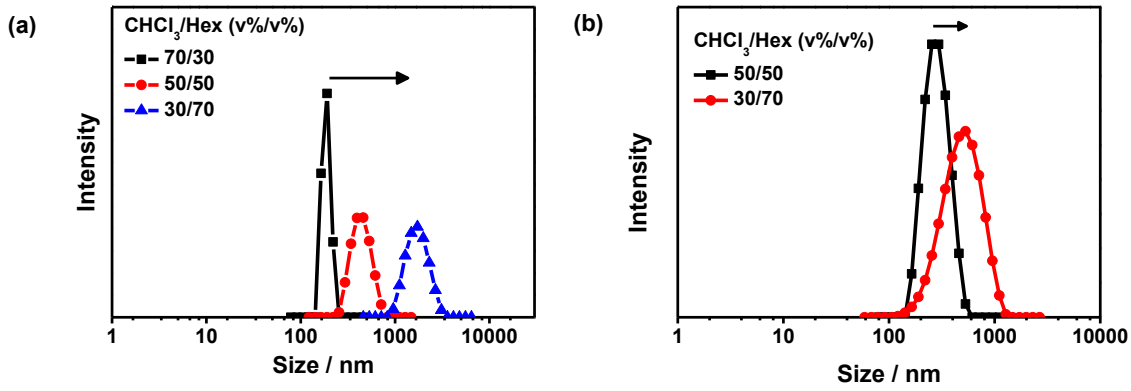

Figure S9 Solvent composition-dependent DLS traces of (a) **1** (8.40 μM) and (b) **2** (5.7 μM) in various *n*-hexane-$CHCl_3$ mixtures.

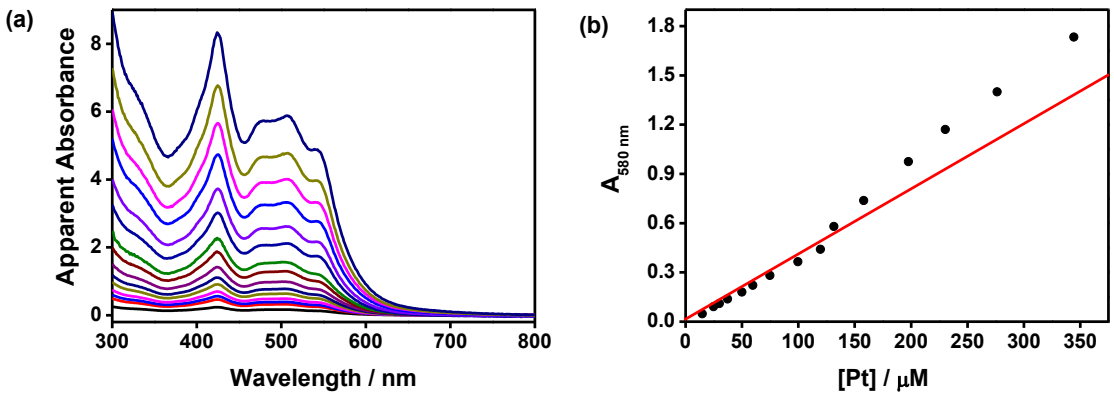

Figure S10 (a) Concentration-dependent UV–vis absorption spectra of **2** in 70% *n*-hexane-$CHCl_3$ with concentration ranges from 3.7 to 86.1 μM. The apparent absorbance values have been obtained by correcting to 1-cm path length equivalence. (b) A plot of absorbance monitored at 580 nm against concentration.

Morphological Studies

Table S5 WAXS data of **1**

Lattice	q / nm^{-1}	d_{obs} / nm	d_{cal} / nm	*hkl*
2D *P6mm*[a] (298 K)	1.81	3.47	3.40	100
	3.65	1.72	1.72	200
	4.91	1.28	1.29	$3\bar{1}0$
	6.48	0.97	0.99	220
	16.98	0.37		–[b]
	17.93	0.35		–[b]

[a]Lattice parameter: a = 4.01 nm. Simulated lattice parameter: a = 3.93 nm. [b]Distance of π···π and Pt···Pt distances.

Table S6 WAXS data of **2**

Lattice	q / nm^{-1}	d_{obs} / nm	d_{cal} / nm	*hkl*
2D *C2lm*[a] (298 K)	2.27	2.76	2.61	200
	4.30	1.46	1.40	020
	5.48	1.15	1.24	220

[a]Lattice parameter: a = 5.52 nm, b = 2.92 nm. Simulated lattice parameter: a = 5.22 nm, b = 2.80 nm.

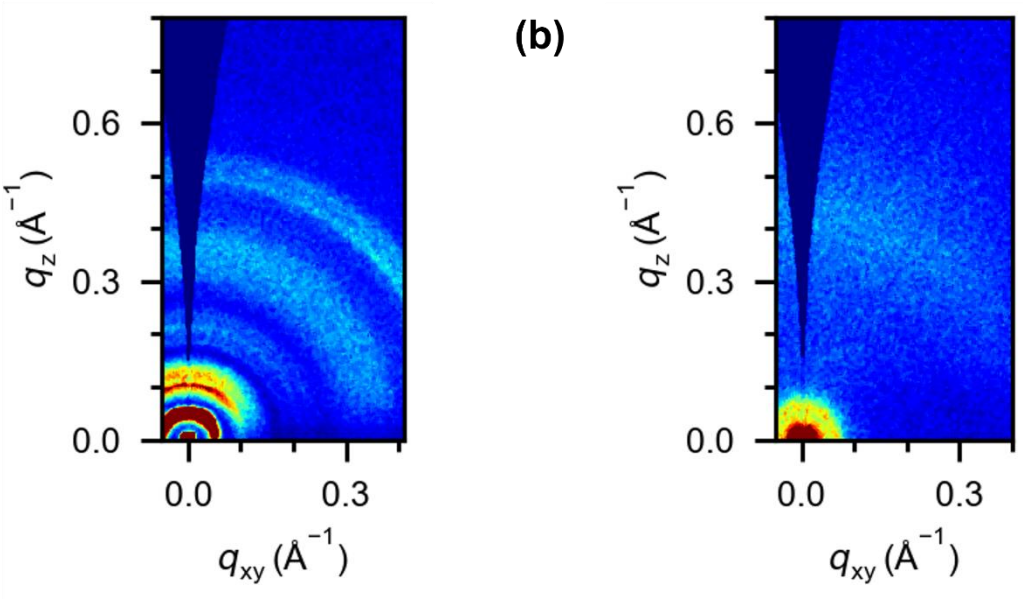

Figure S11 2D GI-XRD image of (a) **1** and (b) **2** drop-casted on silicon wafer.

Supramolecular Self-assembly Studies Upon Addition of PFAS

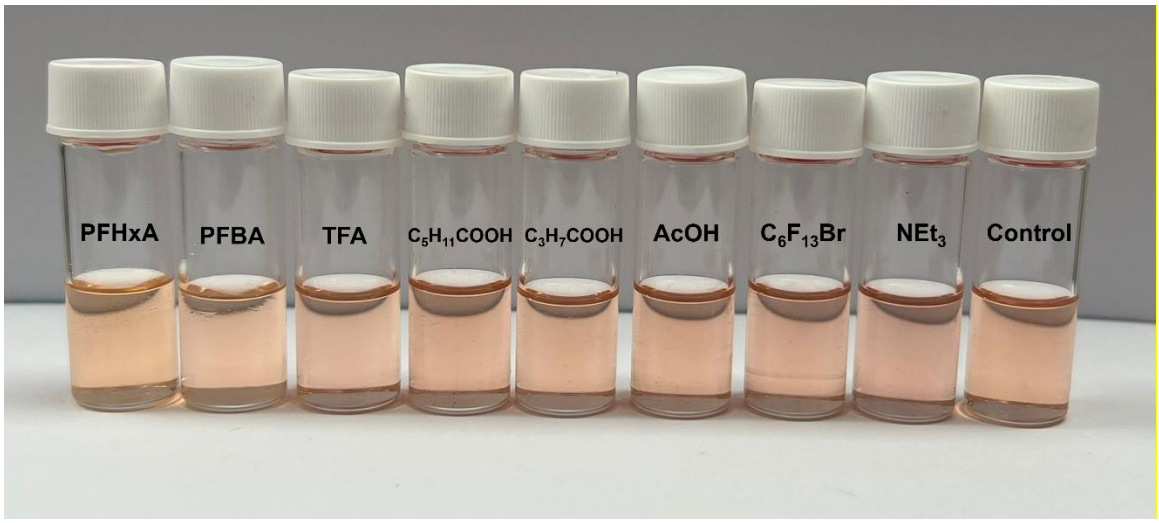

Figure S12 Photographs under nature light of **2** (6.23 μM) in 70% *n*-hexane-$CHCl_3$ upon the addition of various chemicals (187 mM).

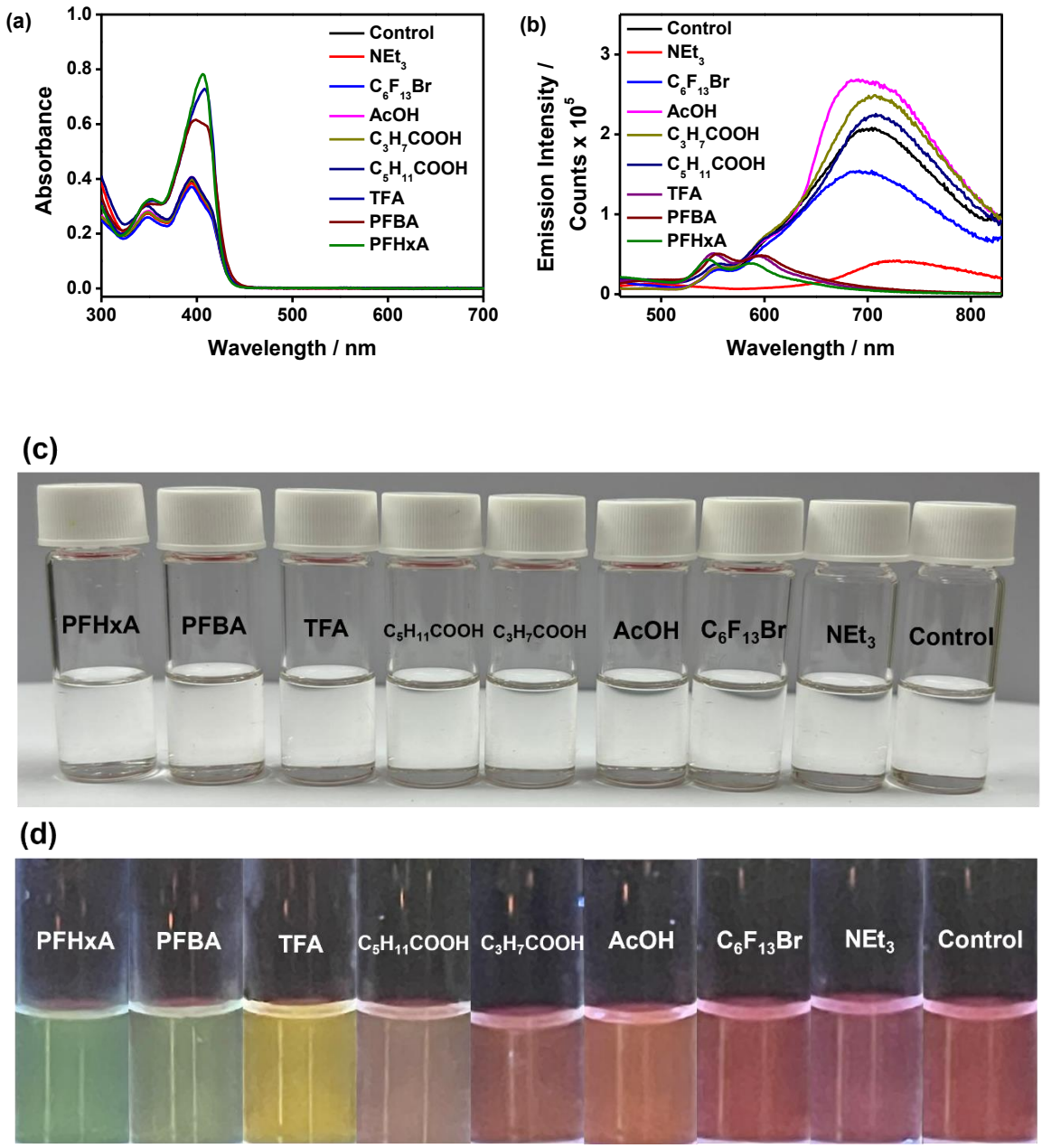

Figure S13 (a) UV–Vis absorption spectra, (b) emission spectra and (c, d) photographs under natural light / UV-light (λ_{ex} = 365 nm) of **1** (8.40 μM) after addition of various chemicals (168 mM) in 70% *n*-hexane-$CHCl_3$.

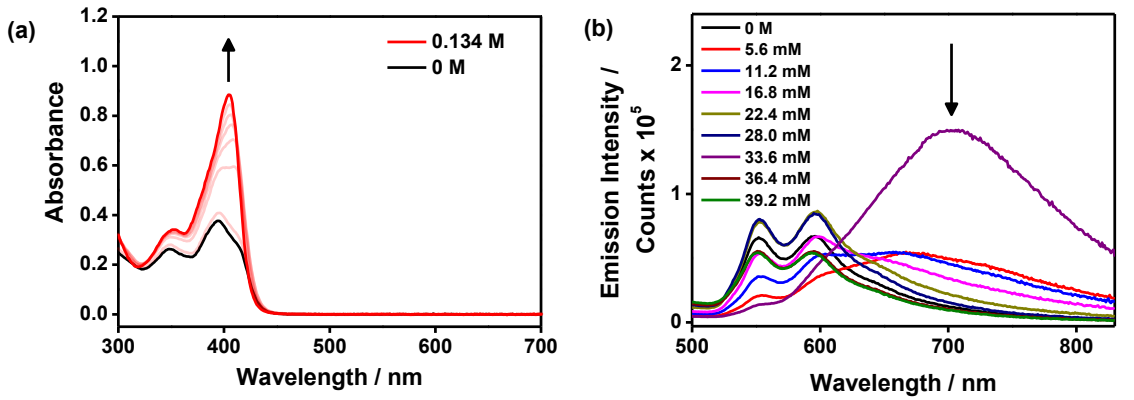

Figure S14 (a) UV–Vis absorption and (b) emission spectral changes of **1** in 70% *n*-hexane-$CHCl_3$ upon addition of PFHxA. The excitation wavelength is 400 nm. The concentration of **1** is 6.72 μM.

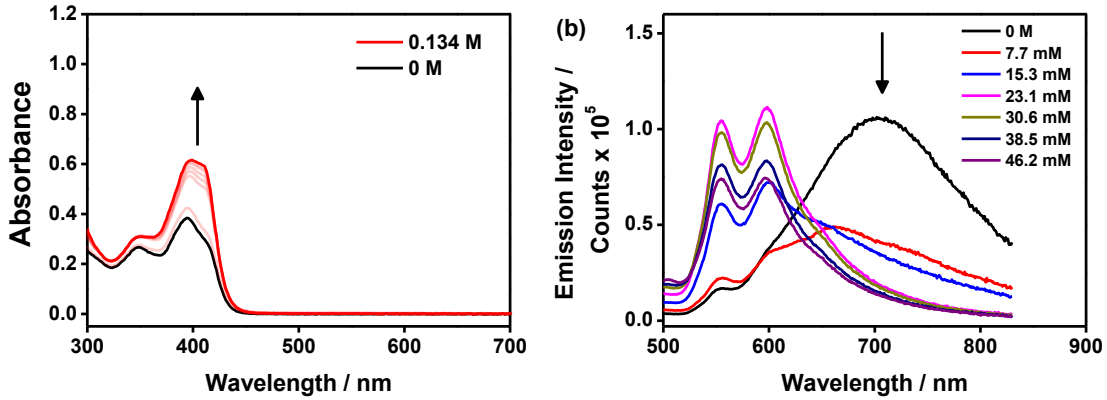

Figure S15 (a) UV–Vis absorption and (b) emission spectral changes of **1** in 70% *n*-hexane-$CHCl_3$ upon addition of PFBA. The excitation wavelength is 400 nm. The concentration of **1** is 6.72 μM.

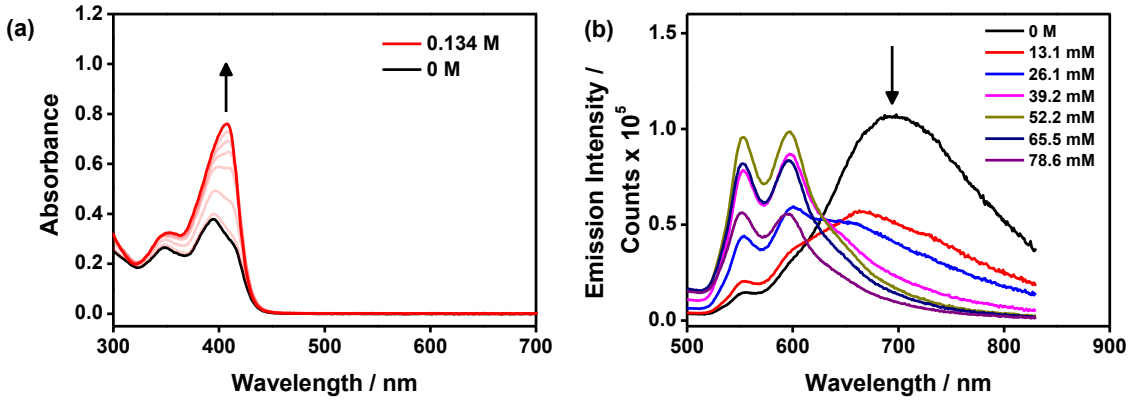

Figure S16 (a) UV–Vis absorption and (b) emission spectral changes of **1** in 70% *n*-hexane-$CHCl_3$ upon addition of TFA. The excitation wavelength is 400 nm. The concentration of **1** is 6.72 μM.

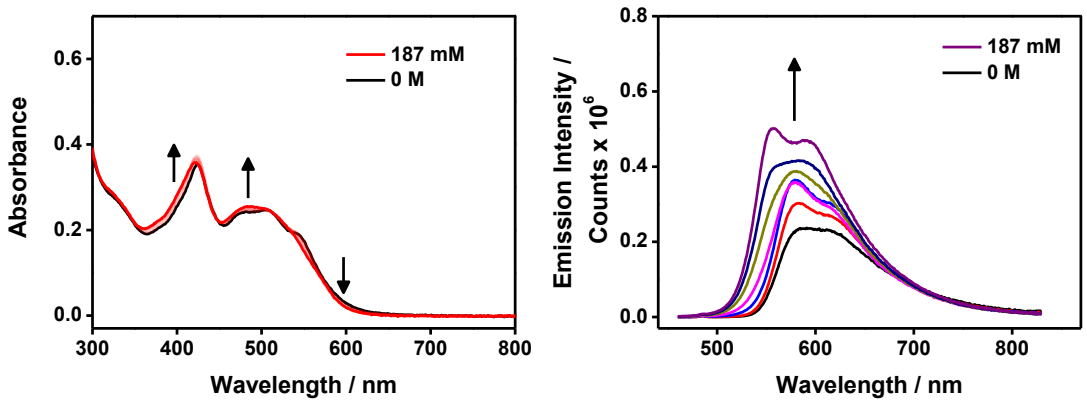

Figure S17 (a) UV–Vis absorption and (b) emission spectral changes of **2** in 70% *n*-hexane-$CHCl_3$ upon addition of PFBA. The excitation wavelength is 425 nm. The concentration of **2** is 6.23 μM.

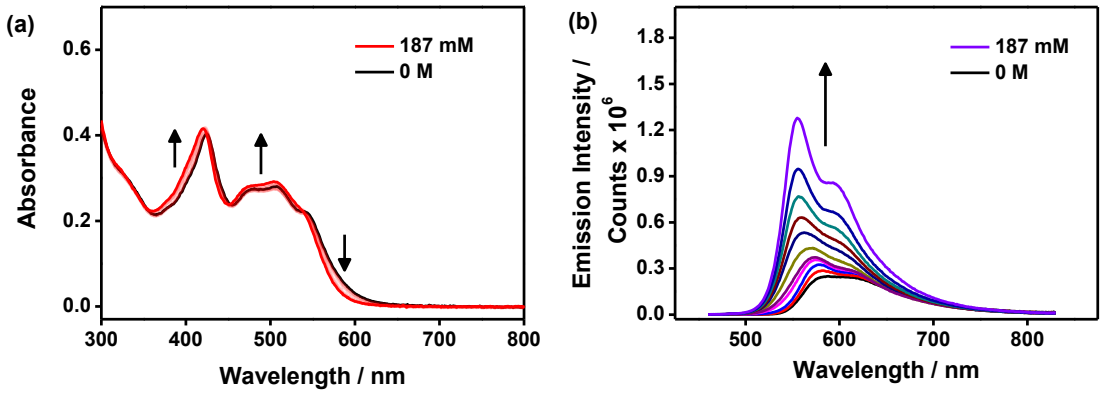

Figure S18 (a) UV–Vis absorption and (b) emission spectral changes of **2** in 70% *n*-hexane-$CHCl_3$ upon addition of TFA. The excitation wavelength is 425 nm. The concentration of **2** is 6.23 μM.

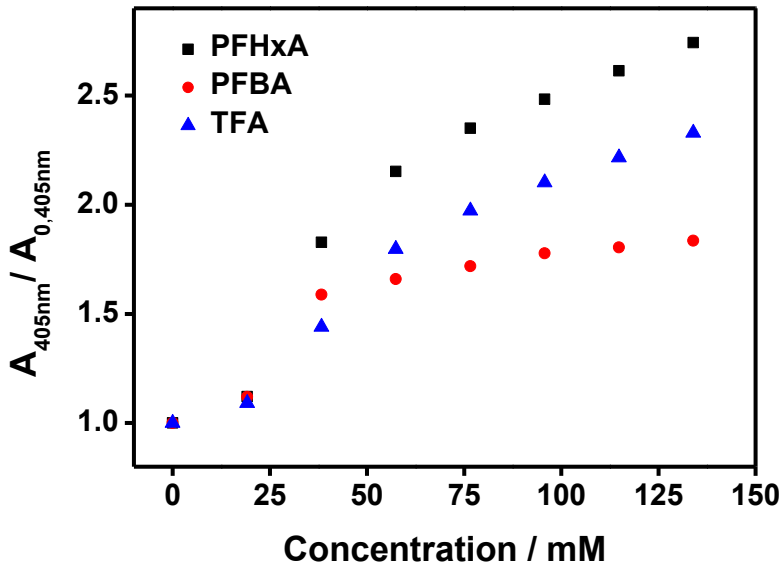

Figure S19 A plot of relative absorbance at 405 nm against concentration of PFAS in a 70% *n*-hexane-$CHCl_3$ solution of **1**. The concentration of **1** is 6.23 μM**.**

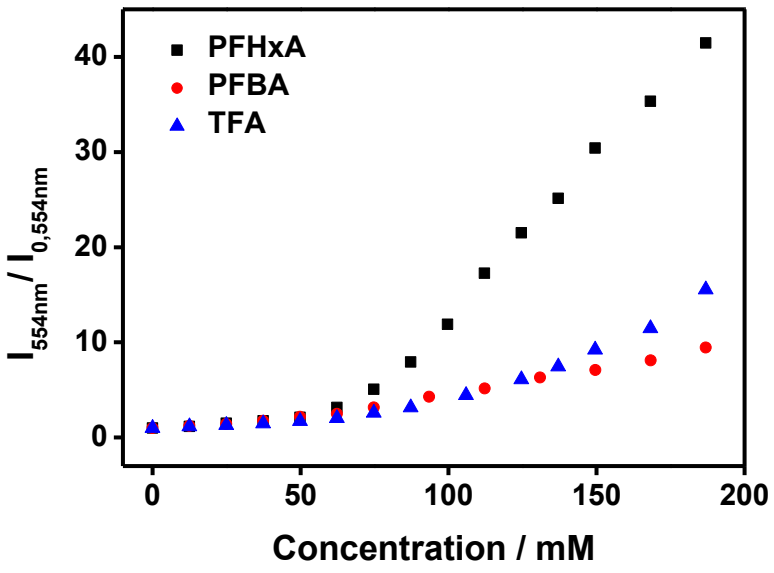

Figure S20 A plot of relative emission intensity at 554 nm against concentration of PFAS in a 70% *n*-hexane-$CHCl_3$ solution of **2**. The concentration of **2** is 6.23 μM.

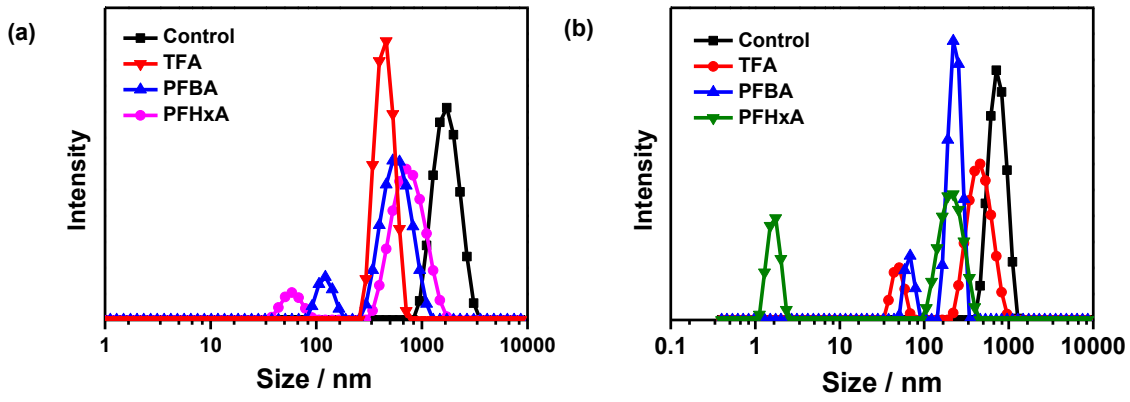

Figure S21 DLS traces of (a) **1** (8.40 μM) and (b) **2** (6.23 μM) in 70% *n*-hexane-$CHCl_3$ upon addition of PFAS.

Molecular Dynamics Simulations

Molecular Dynamics Simulations. General amber force field (GAFF) parameters were used to describe the bonded and non-bonded interactions in solvent molecules and OTf counterion.[14] For the complex cation **3**, the bonded interactions involving platinum center were obtained using the modified Seminario method,[15] which derives accurate harmonic bond, angle and dihedral angle parameters directly from the PBE0-D3BJ computed Hessian matrix. The bonded interactions in the organic part that does not involve Pt were described by GAFF. In addition, GAFF was also applied to describe the non-bonded interactions for the non-metal part in **3**. The Lennard-Jones parameters [σ(Pt) = 0.33298 nm and ε(Pt) = 5.267 kJ mol^{-1}] for platinum were taken from our previous work to properly model the metal–metal interactions in the self-assembly process.[16, 17] RESP atomic charges computed at PBE0-D3BJ level were used. All topology files were generated by Sobtop (version 1.0, dev5) package.[18]

All MD simulations were performed using GROMACS (version 2021.3) package.[19] The initial configurations were generated randomly placing 10 complex cations, 10 OTf$^-$ counter anions, and other species specified in Table S7 in a cubic simulation box with an edge length of 16 nm. The energy minimization was performed (maximal force F_{max} < 100 kJ mol^{-1} nm^{-1} on each atom), followed by a 2-ns equilibrium simulation under the NPT (298 K, 1 atm) ensemble using V-rescale thermostat and Berendsen barostat (isothermal compressibility κ = 1.2 × 10^{-4} bar^{-1}) with the coupling time constant of 0.2 and 2 ps, respectively. The temperature T was increased from 0 to 298 K during the initial 1 ns of the simulation, and then T was maintained at 298 K. The long-range electrostatic interactions beyond the cutoff at 10 Å were considered using the particle-mesh Ewald (PME) method, and the integration time step was 2 fs. Finally, a 300-ns production simulation was performed under the NPT (298 K, 1 atm) ensemble using V-rescale thermostat and Parrinello-Rahman barostat (κ = 1.2 × 10^{-4} bar^{-1}) with the coupling time constant of 0.2 and 2 ps, respectively. The integration time step was set to 2 fs in the production simulation. The pairwise radial distribution function (RDF) $g_{Pt–Pt}(r)$ records the distribution of Pt···Pt distances. The dominant peak indicates the presence of a dimeric aggregate as well as dimeric structures within a higher-order aggregate. The intensity of

the first $g_{Pt–Pt}(r)$ peak was monitored over the simulation time t (Figure S23). It is found that the intensity of the first peak becomes stable when $t > 200$ ns. Thus, RDF curves reported in this work were prepared using the MD trajectory from 250–300 ns. The replicated simulations with different initial configurations (Figure S25) have been conducted, and consistent results could be derived.

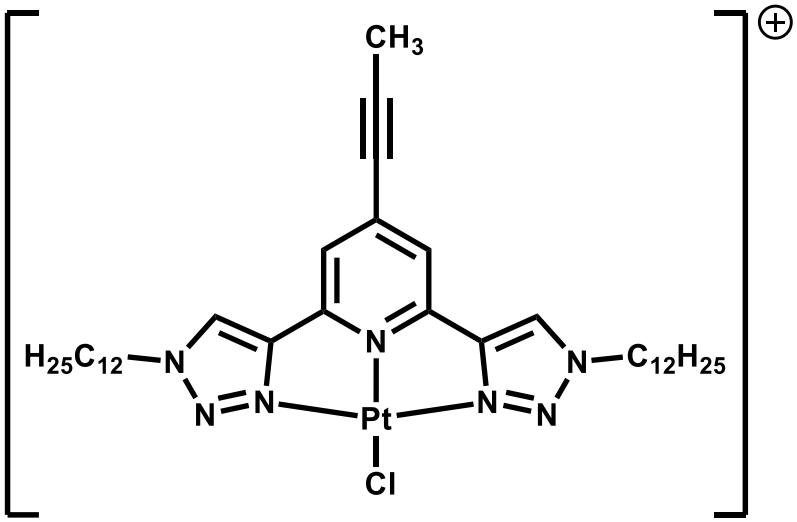

Figure S22 Molecular structure of model complex cation **3**.

Table S7 Molecular species in four solution environments (10 complex cations and 10 OTf^- anions are included during the simulation)

	Components
Control	3300 $CHCl_3$, and 7700 *n*-hexane
$C_5F_{11}COOH$	1000 $C_5F_{11}COOH$, 3000 $CHCl_3$, and 7000 *n*-hexane
$C_5H_{11}COOH$	1000 $C_5H_{11}COOH$, 3000 $CHCl_3$, and 7000 *n*-hexane
$C_6F_{13}Br$	1000 $C_6F_{13}Br$, 3000 $CHCl_3$, and 7000 *n*-hexane

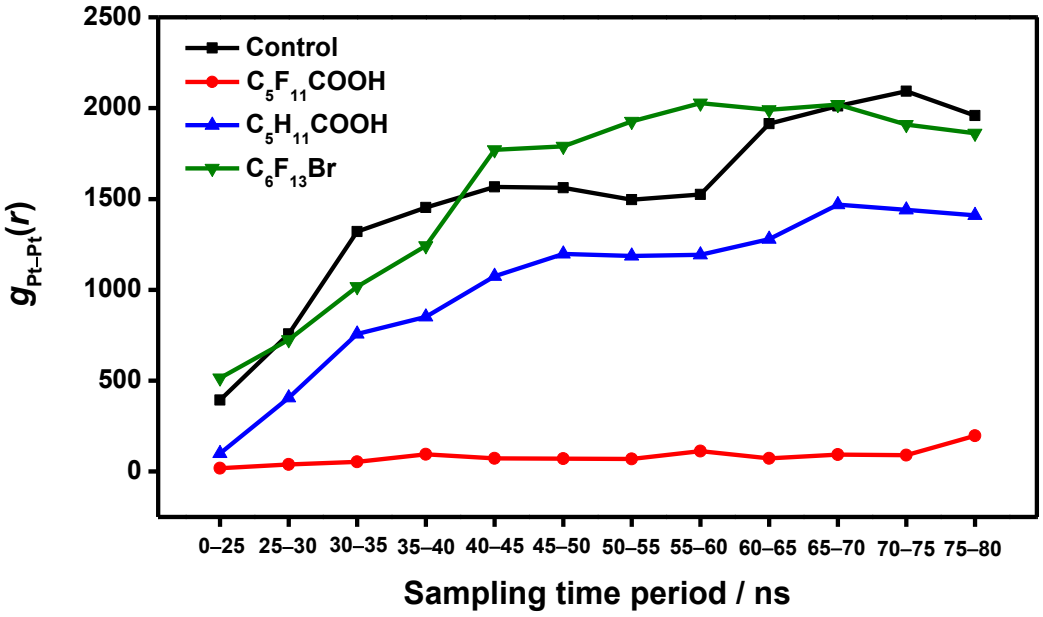

Figure S23 The intensity of the first $g_{Pt-Pt}(r)$ peak as a function of simulation time.

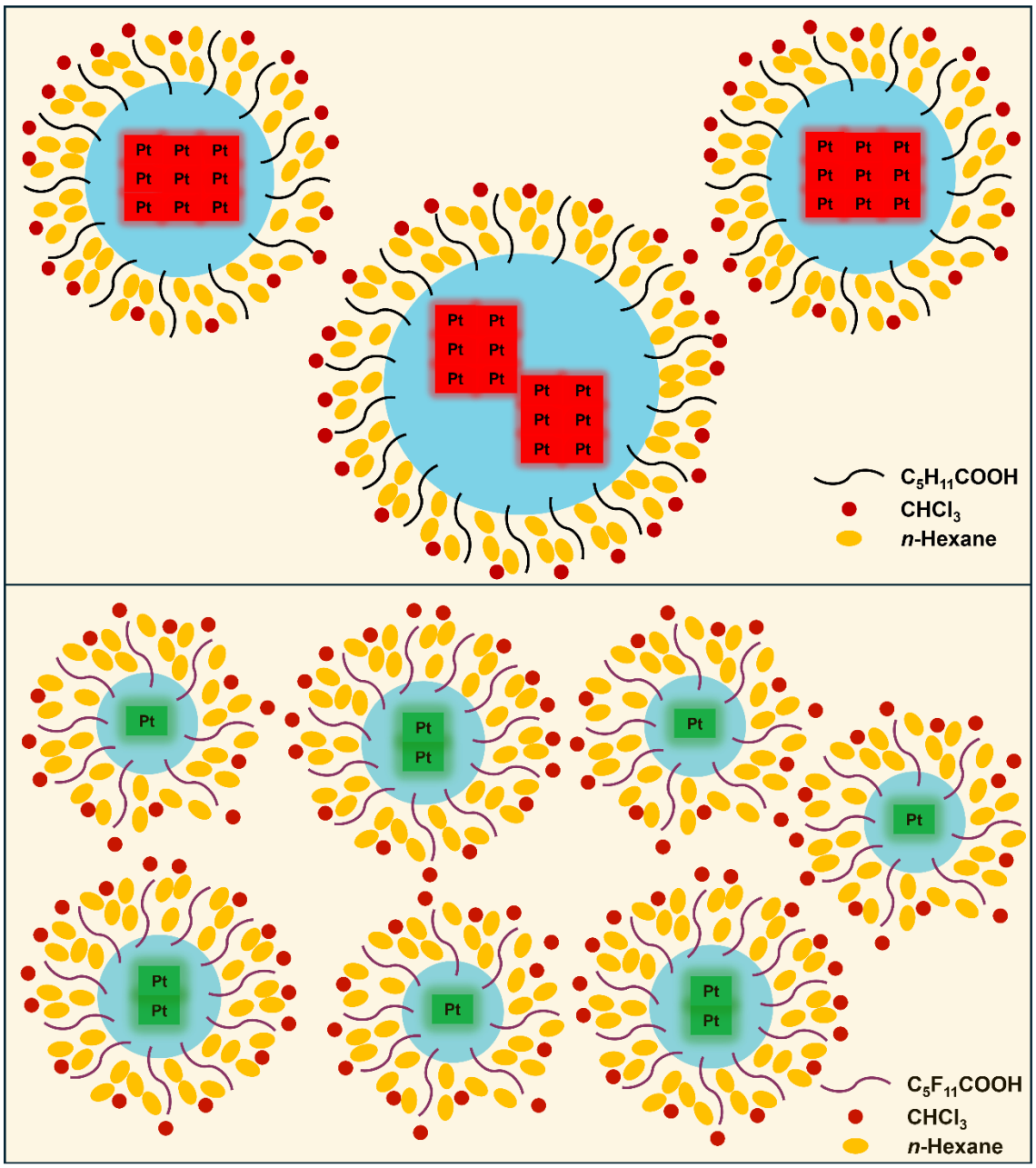

Figure S24 Proposed self-assembly behavior of **1** and **2** in 70% *n*-hexane-$CHCl_3$ in the presence of $C_5H_{11}COOH$ (top) or $C_5F_{11}COOH$ (bottom).

Table S8 Cartesian coordinates of the optimized S_0 structure of **3**

1	C	–1.061693	–2.868173	0.426755	**52**	H	–13.095051	1.396223	–1.340338
2	C	1.076235	–2.688649	–0.571711	**53**	C	–14.358954	2.719992	–0.205703
3	C	1.156001	–4.062553	–0.723692	**54**	H	–14.800588	1.931824	0.420612
4	C	0.086275	–4.861853	–0.276687	**55**	H	–14.248733	3.597773	0.446723
5	C	–1.039069	–4.246692	0.304377	**56**	C	–15.315502	3.054266	–1.343937
6	H	2.026212	–4.524110	–1.174419	**57**	H	–14.874666	3.842808	–1.970474
7	H	–1.869556	–4.848818	0.651860	**58**	H	–15.424764	2.176508	–1.996940
8	C	2.048623	–1.670176	–0.946318	**59**	C	–16.693113	3.501305	–0.868091
9	C	3.280659	–1.621263	–1.553377	**60**	H	–17.130975	2.713211	–0.240829
10	H	3.933035	–2.384768	–1.947089	**61**	H	–16.582499	4.379038	–0.217293
11	C	–2.106296	–2.020467	0.985533	**62**	C	–17.640910	3.829490	–2.014042
12	C	–3.358328	–2.182208	1.530055	**63**	H	–18.622041	4.147074	–1.647974
13	H	–3.967902	–3.052368	1.716967	**64**	H	–17.240779	4.636658	–2.637593
14	N	–0.015615	–2.133581	–0.005457	**65**	H	–17.792849	2.958675	–2.661415
15	N	–1.862598	–0.666810	1.004131	**66**	C	4.817807	0.318727	–2.078473
16	N	–2.858946	–0.015795	1.510715	**67**	H	5.068986	–0.152854	–3.032330
17	N	–3.761658	–0.928711	1.833682	**68**	H	4.563335	1.363182	–2.268162
18	N	1.719106	–0.364533	–0.663966	**69**	C	5.953883	0.196561	–1.073666
19	N	2.647304	0.449400	–1.050513	**70**	H	6.165346	–0.863969	–0.885571
20	Pt	–0.079374	–0.164344	0.216835	**71**	H	5.633144	0.634971	–0.121342
21	Cl	–0.151821	2.116705	0.485290	**72**	C	7.211577	0.896220	–1.575344
22	C	0.142695	–6.270162	–0.406235	**73**	H	7.511175	0.468020	–2.541653
23	C	0.190057	–7.477403	–0.510111	**74**	H	6.987509	1.954611	–1.764016
24	C	0.245817	–8.920048	–0.632360	**75**	C	8.372150	0.791909	–0.593018
25	H	0.167813	–9.392246	0.352225	**76**	H	8.597972	–0.267268	–0.406344
26	H	–0.581780	–9.286842	–1.247922	**77**	H	8.067615	1.214454	0.374172
27	H	1.185118	–9.239065	–1.093014	**78**	C	9.629515	1.500544	–1.081607
28	N	3.589828	–0.306043	–1.592612	**79**	H	9.932624	1.078811	–2.050217
29	C	–5.060638	–0.496161	2.343039	**80**	H	9.399342	2.558395	–1.270225
30	H	–5.445089	–1.309579	2.962736	**81**	C	10.793172	1.404664	–0.102421
31	H	–4.869687	0.366183	2.984944	**82**	H	11.025724	0.346770	0.084997
32	C	–6.012929	–0.149442	1.207515	**83**	H	10.487993	1.823864	0.866649
33	H	–6.136945	–1.026775	0.559934	**84**	C	12.048281	2.119481	–0.588207
34	H	–5.557284	0.638610	0.596530	**85**	H	11.813501	3.176443	–0.777577
35	C	–7.369165	0.311092	1.728366	**86**	H	12.354100	1.699840	–1.557056
36	H	–7.814072	–0.477909	2.350198	**87**	C	13.212843	2.029789	0.390551
37	H	–7.232959	1.181450	2.384061	**88**	H	13.449197	0.972928	0.579375
38	C	–8.330096	0.670151	0.600840	**89**	H	12.906108	2.448407	1.359544
39	H	–8.455521	–0.199082	–0.059744	**90**	C	14.466245	2.748149	–0.094619
40	H	–7.883495	1.460729	–0.017470	**91**	H	14.228499	3.804380	–0.285014
41	C	–9.696119	1.127407	1.097699	**92**	H	14.773658	2.328840	–1.063198
42	H	–10.140792	0.338219	1.720204	**93**	C	15.630928	2.662568	0.884300
43	H	–9.572127	1.999278	1.754929	**94**	H	15.323733	3.081749	1.853102
44	C	–10.654614	1.478284	–0.033962	**95**	H	15.869918	1.606492	1.075032
45	H	–10.772017	0.606495	–0.693218	**96**	C	16.884353	3.382418	0.399612
46	H	–10.209925	2.268808	–0.654681	**97**	H	16.643093	4.436667	0.208384
47	C	–12.026623	1.930272	0.451292	**98**	H	17.189929	2.962122	–0.567979
48	H	–12.469881	1.141528	1.075612	**99**	C	18.041506	3.292642	1.385565
49	H	–11.911445	2.805418	1.106185	**100**	H	18.928433	3.816061	1.015591
50	C	–12.983522	2.271541	–0.684664	**101**	H	17.771995	3.735406	2.350844
51	H	–12.540551	3.061004	–1.308211	**102**	H	18.322730	2.249773	1.569480

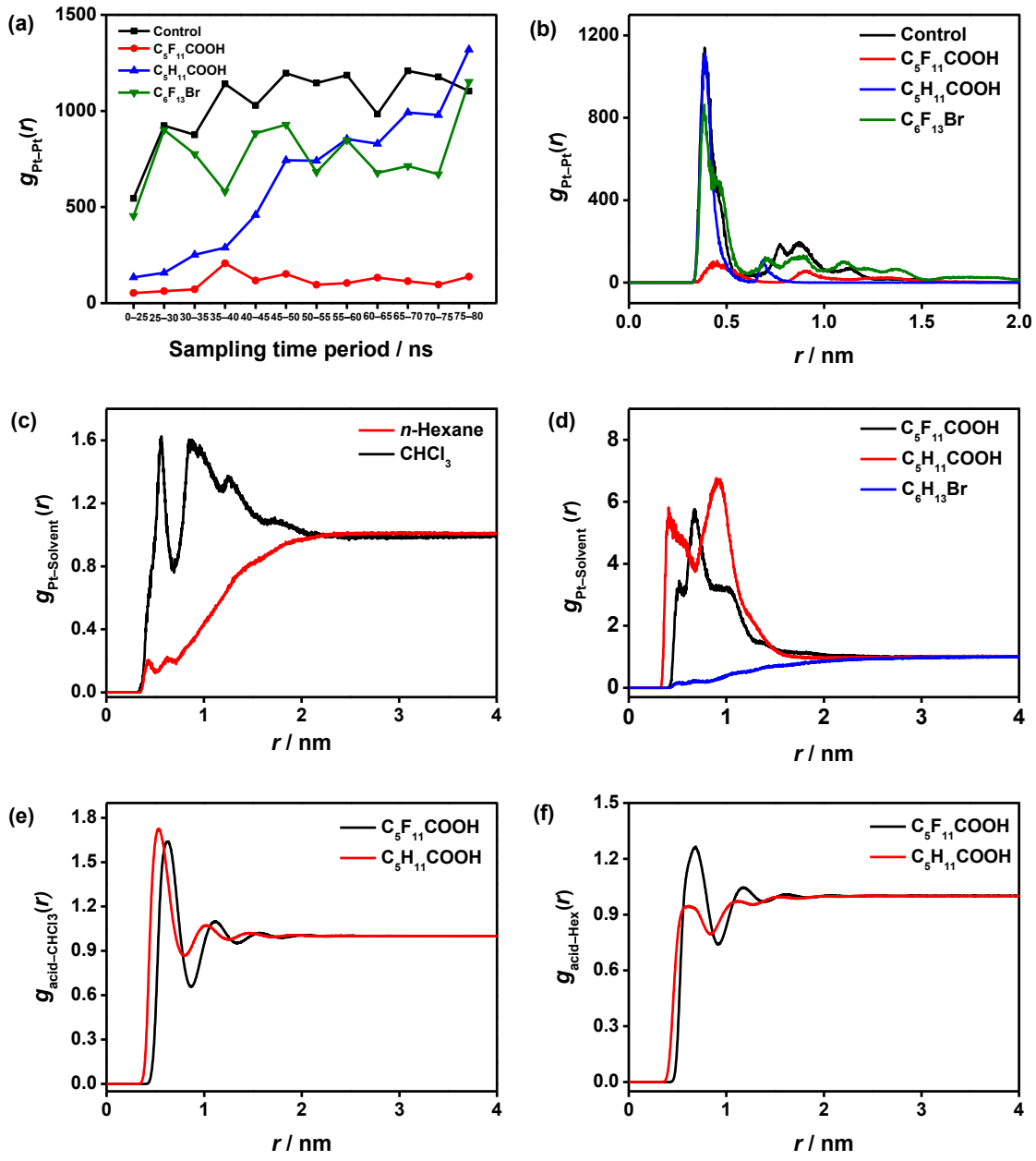

Figure S25 Replicated MD simulations for **3** with different initial configurations. (a) The intensity of the first $g_{Pt–Pt}(r)$ peak as a function of simulation time. (b) RDF $g_{Pt–Pt}(r)$ for the complex cation **3**. (c, d) RDF $g_{Pt–solvent}(r)$ between **3** and solvent molecules (*n*-hexane, $CHCl_3$, $C_5F_{11}COOH$, $C_5H_{11}COOH$ and $C_6F_{13}Br$). (e, f) RDF $g_{acid–solvent}(r)$ between $C_5F_{11}COOH$/$C_5H_{11}COOH$ and $CHCl_3$/*n*-hexane.

Extraction of PFAS from Aqueous Phase

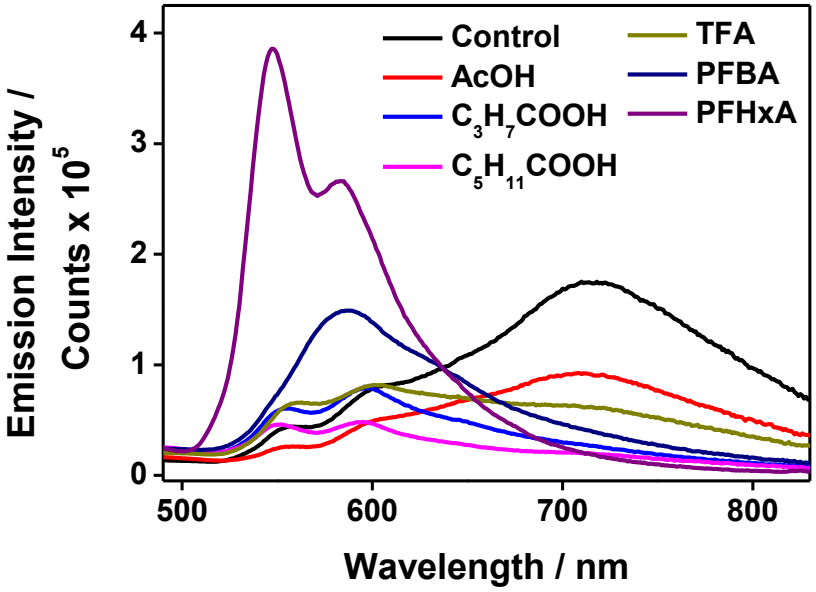

Figure S26 Emission spectra of **1** in 70% *n*-hexane-$CHCl_3$ (8.40 μM, 2 mL) after extraction with various chemicals in deionized water (100 mM, 2 mL). The excitation wavelength is 400 nm.

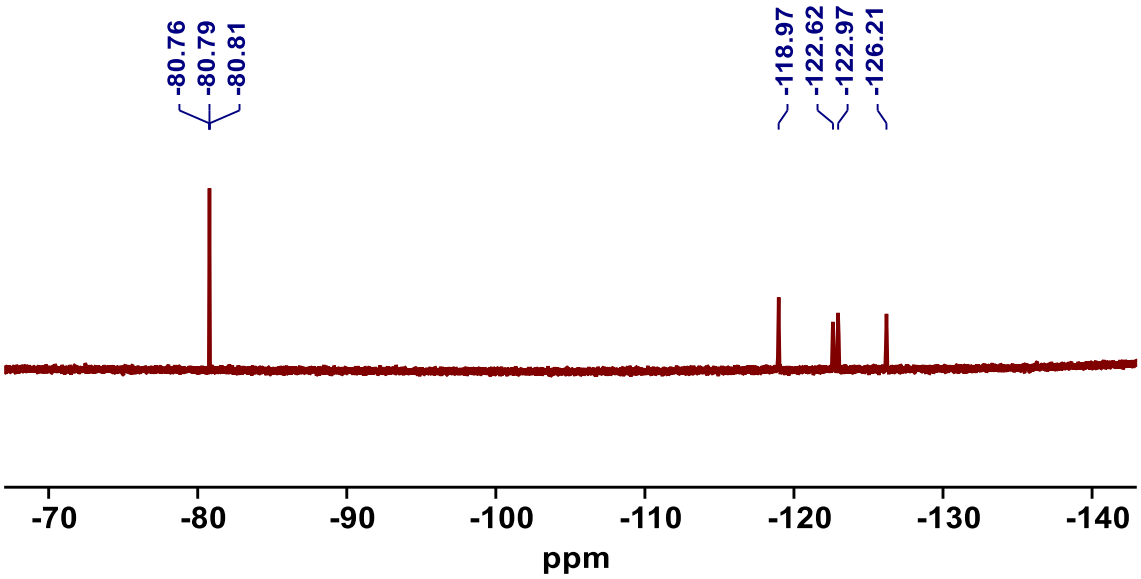

Figure S27 $^{19}F\{H\}$ NMR spectrum of the organic phase containing **1** (8.40 µM) in 70% hexane-$CHCl_3$ (2 mL) after extraction with PFHxA (125 mM) in deionized water (2 mL).

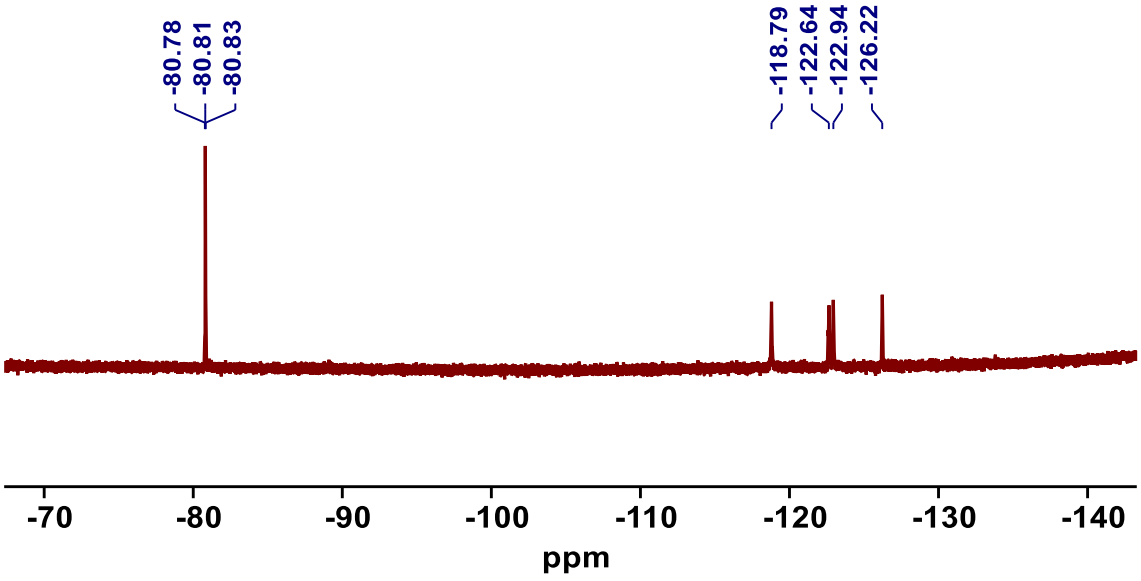

Figure S28 $^{19}F\{H\}$ NMR spectrum of the organic phase containing **2** (6.23 µM) in 70% *n*-hexane-$CHCl_3$ (2 mL) after extraction with PFHxA (125 mM) in deionized water (2 mL).

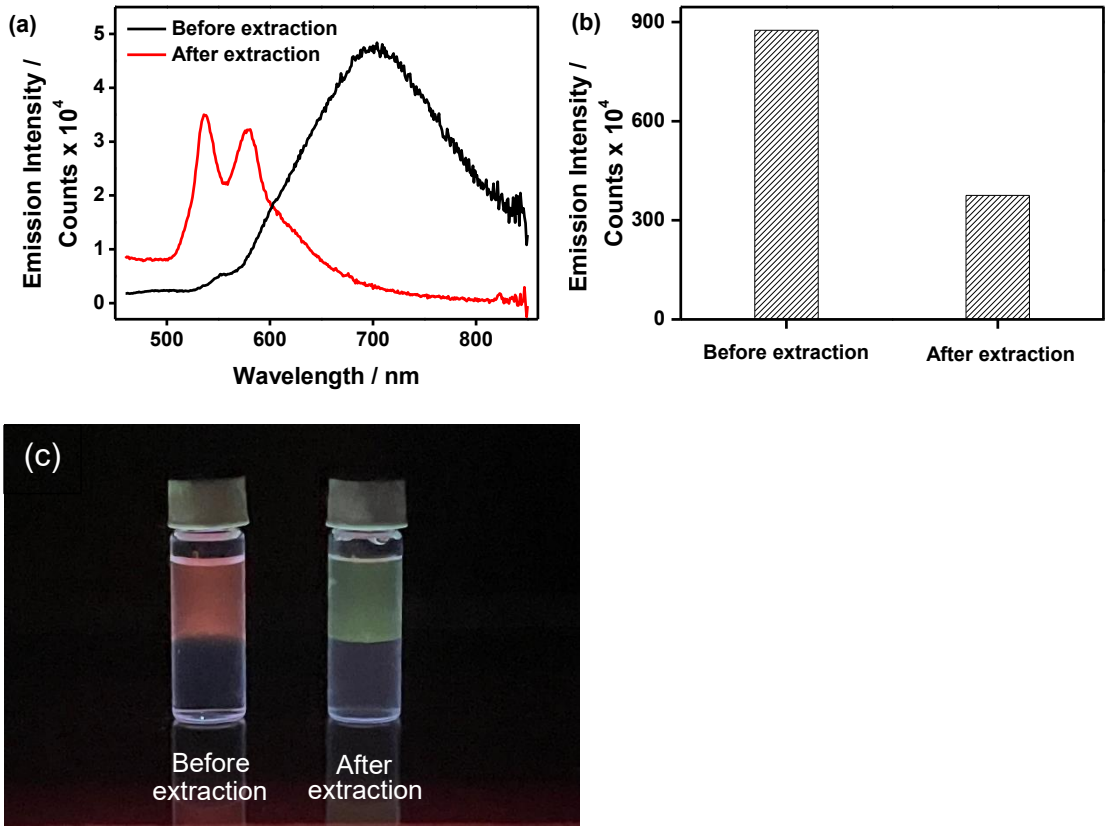

Figure S29 (a) Emission spectral changes, (b) emission intensity and (c) photographs under UV-light source (λ_{ex} = 365 nm) of **1** (8.40 μM)) in 70% *n*-hexane-$CHCl_3$ (2 mL) before and after extraction with PFHxA in deionized water (2 mL).

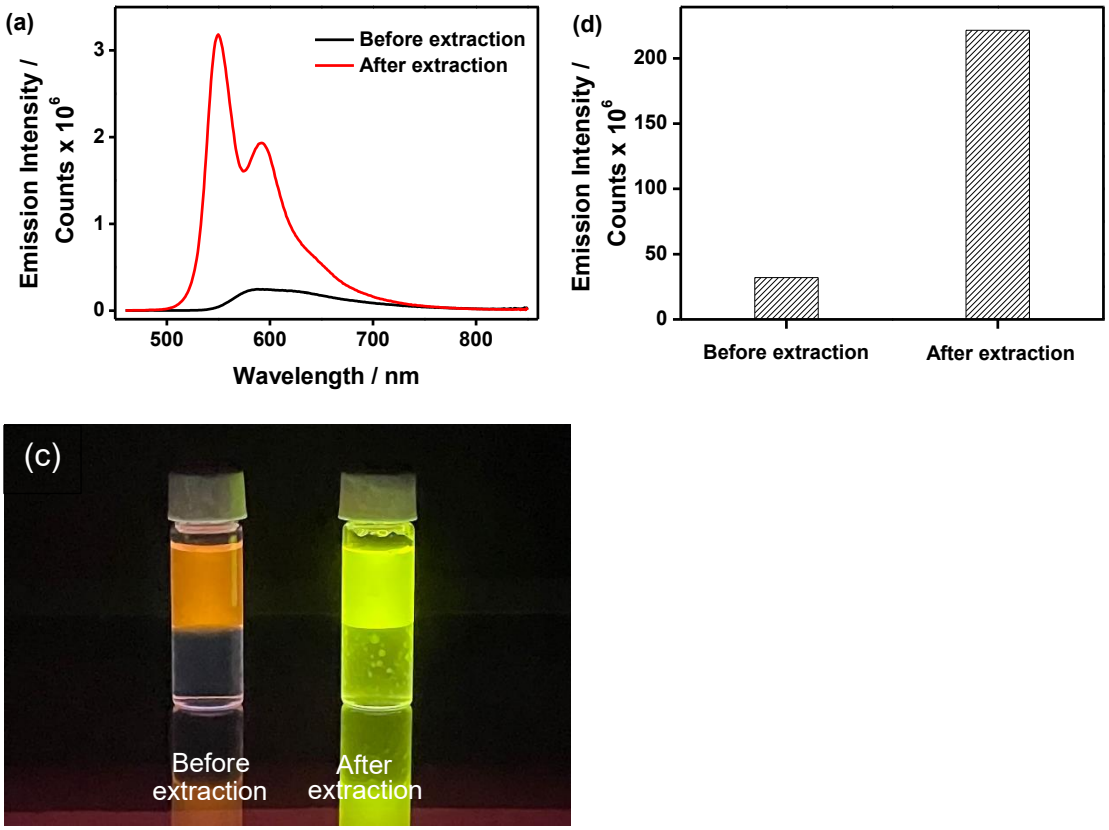

Figure S30 (a) Emission spectral changes, (b) emission intensity (area under curve) and (c) photographs under UV-light source (λ_{ex} = 365 nm) of **2** (8.40 μM) in 70% *n*-hexane-$CHCl_3$ (2 mL) before and after extraction with PFHxA in deionized water (2 mL).

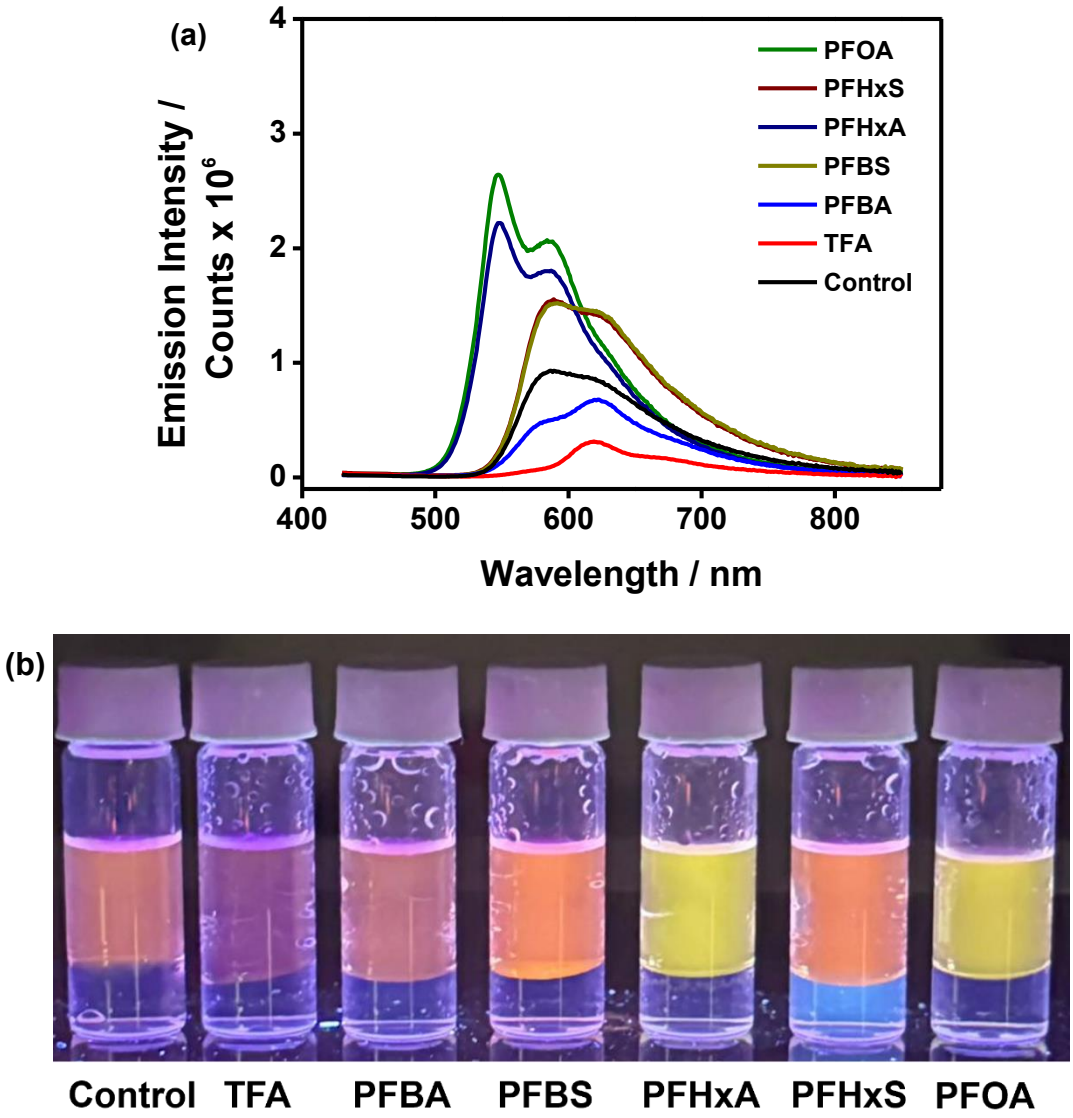

Figure S31 (a) Emission spectra of **2** in 70% *n*-hexane-$CHCl_3$ (1.25 μM, 2 mL) after extraction with various PFAS in deionized water (12.5 mM, 1 mL). The excitation wavelength is 425 nm. (b) Photographs under a UV-light source (λ_{ex} = 365 nm) of **2** (1.25 μM) in 70% *n*-hexane-$CHCl_3$ (2 mL) after extraction with various PFAS in deionized water (1 mL).

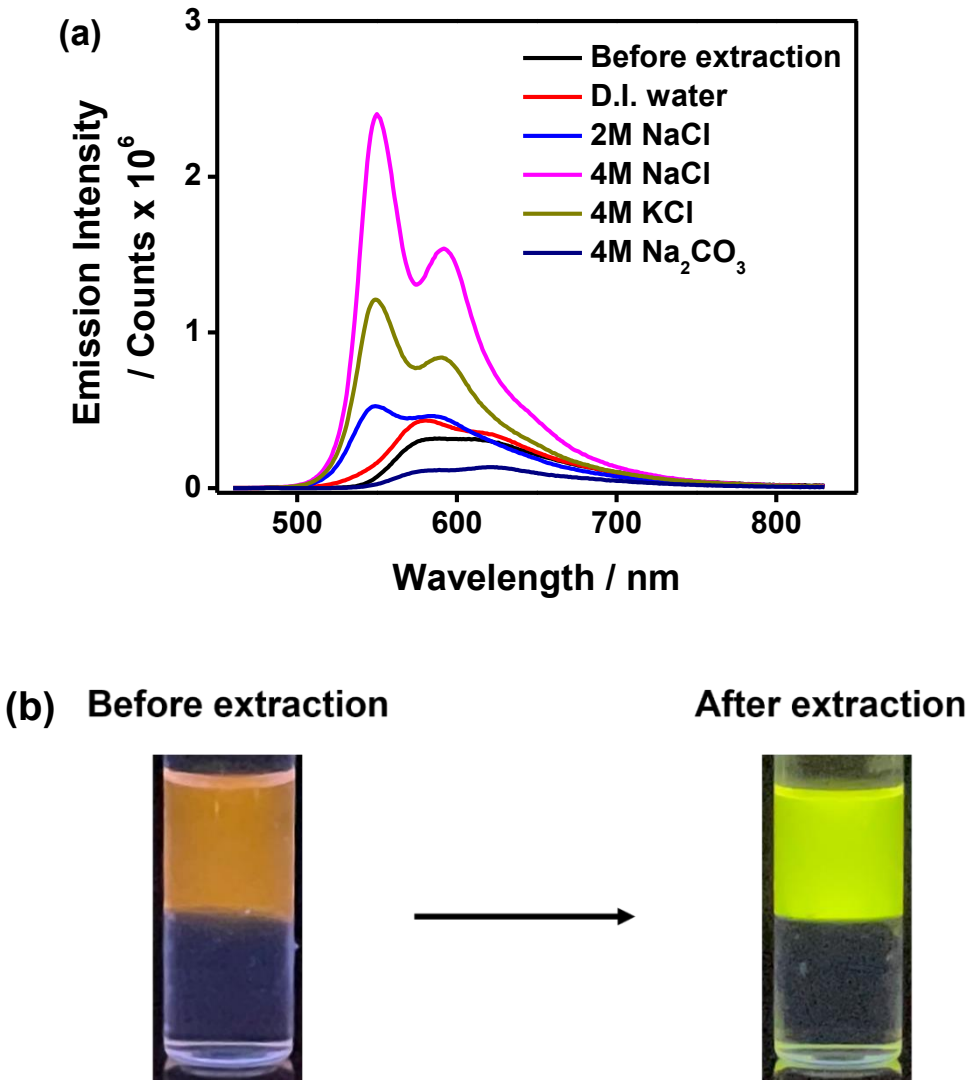

Figure S32 (a) Emission spectra of **2** (6.23 μM) in 70% *n*-hexane-$CHCl_3$ (2 mL) before and after extraction with PFBA (125 mM) in different aqueous media (2 mL; Red line: D.I. water; Blue line: 2M NaCl; Dark yellow line: 4M KCl; Navy line: 4M Na_2CO_3). The excitation wavelength is 425 nm. (b) A photograph of **2** (6.23 μM) in 70% *n*-hexane-$CHCl_3$ (2 mL) under UV-light source (λ_{ex} = 365 nm) before and after extraction with PFBA in 4M NaCl solution (0.125 M, 2 mL).

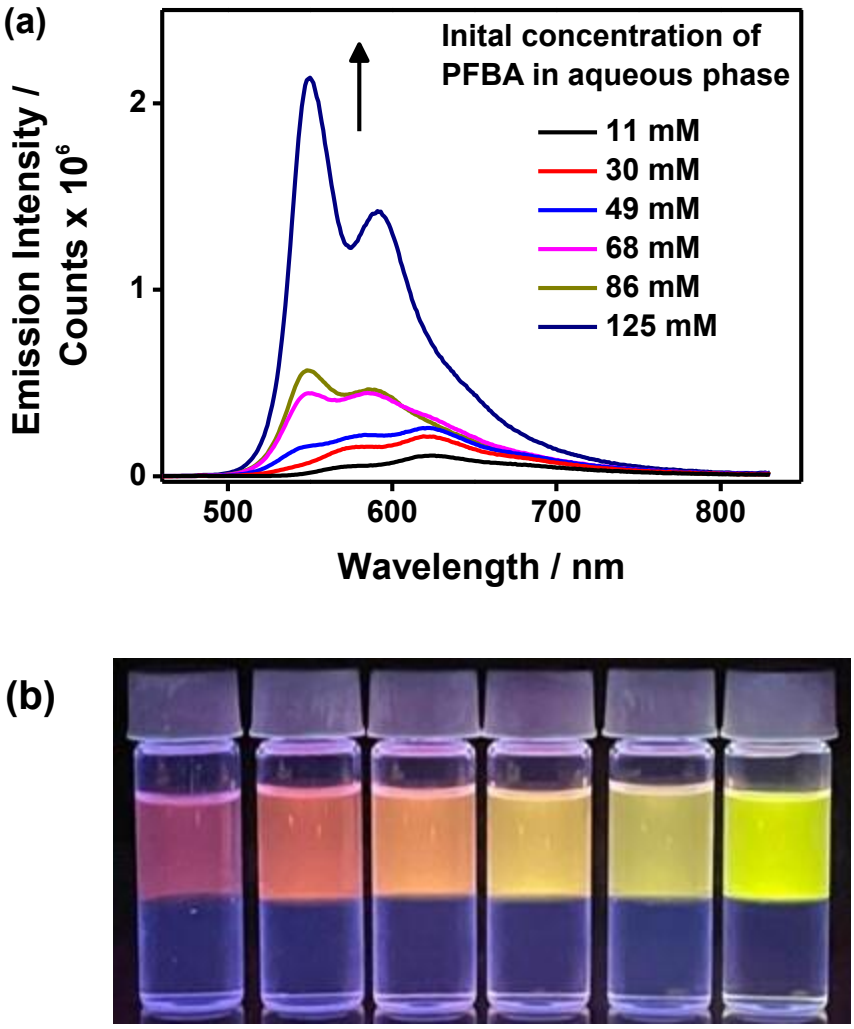

Figure S33 (a) Emission spectra of **2** (6.23 μM) in 70% *n*-hexane-$CHCl_3$ (2 mL) after extraction with different concentrations of PFBA in 4M NaCl (2 mL). The excitation wavelength is 425 nm. (b) A photograph of **2** ((6.23 μM) in 70% *n*-hexane-$CHCl_3$ (2 mL) under UV light source (λ_{ex} = 365 nm) after extraction with PFBA at various concentration in 4M NaCl (2 mL). The concentration of PFBA in the aqueous phase from left to right: 11 mM, 30 mM, 49 mM, 68 mM, 86 mM, 125 mM.

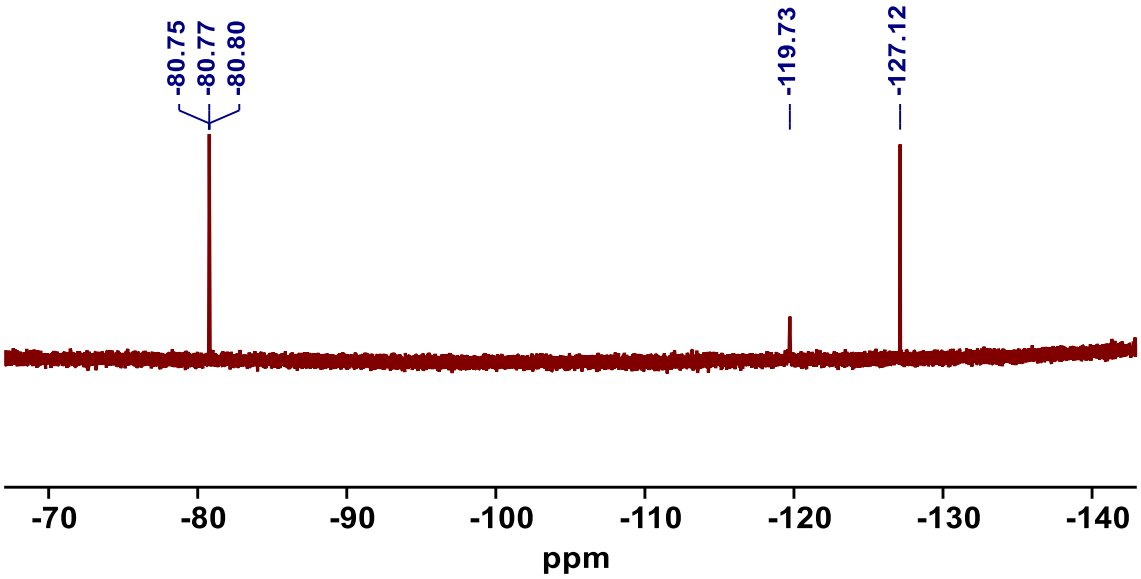

Figure S34 $^{19}F\{H\}$ NMR spectrum of the organic phase containing **2** (6.23 µM) in 70% *n*-hexane-$CHCl_3$ (2 mL) after extraction with PFBA (125 mM) in 4M NaCl (2 mL).

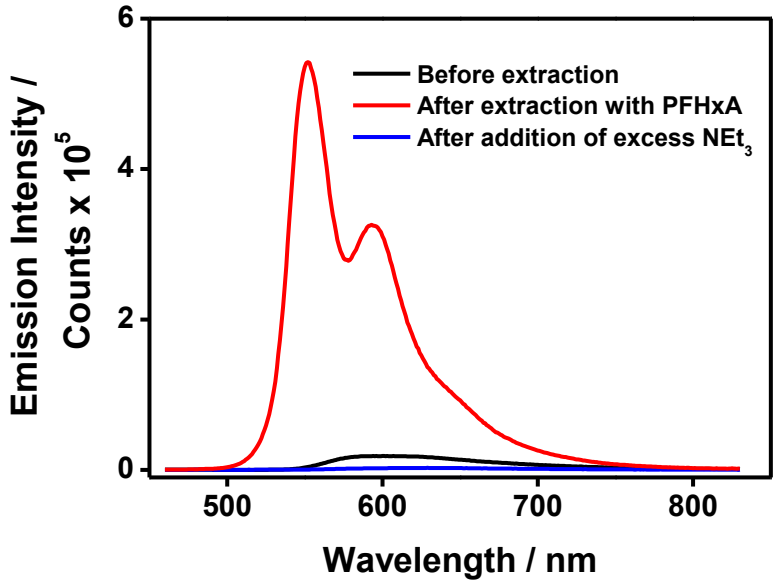

Figure S35 Emission spectra of **2** (6.23 μM) in 70% *n*-hexane-$CHCl_3$ (2 mL) before (black line) and after (red line) extraction with PFHxA (84 mM) in deionized water (2 mL), and the emission spectra of the organic phase (blue line) upon addition of excess NEt_3.

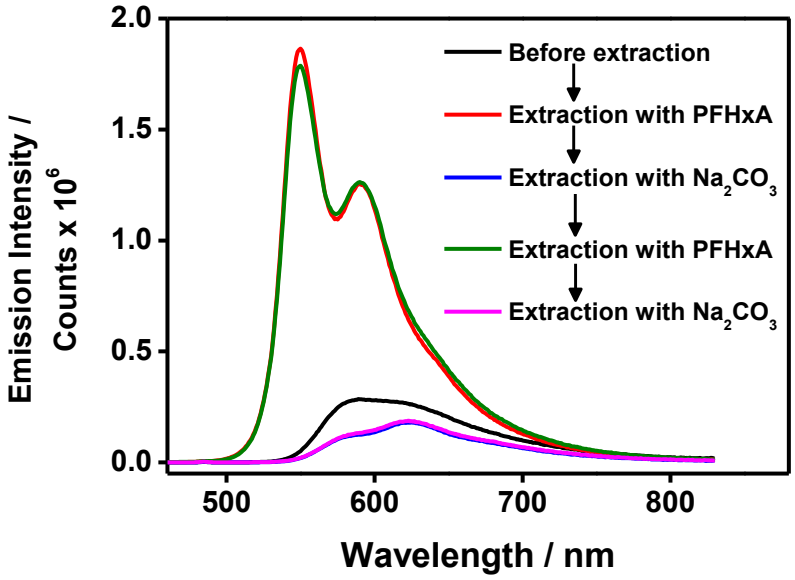

Figure S36 Emission spectral changes of the organic phase containing **2** (6.23 μM) in 70% *n*-hexane-$CHCl_3$ (2 mL) following sequential extraction with PFHxA (84 mM in 2 mL deionized water) and 2 M Na_2CO_3 (2 mL). The excitation wavelength is 425 nm.

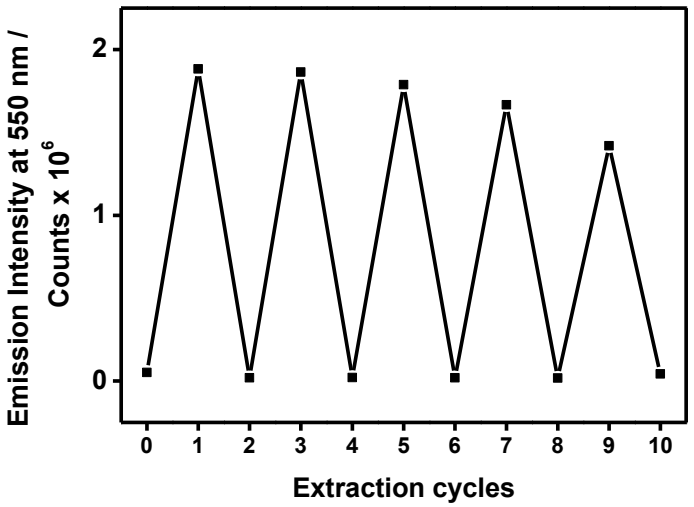

Figure S37 Emission intensity changes of the organic phase containing **2** (6.23 μM) in 70% *n*-hexane-$CHCl_3$ (2 mL) following sequential extraction with PFHxA (84 mM in 2 mL deionized water) and 2 M Na_2CO_3 (2 mL). The excitation wavelength is 425 nm.

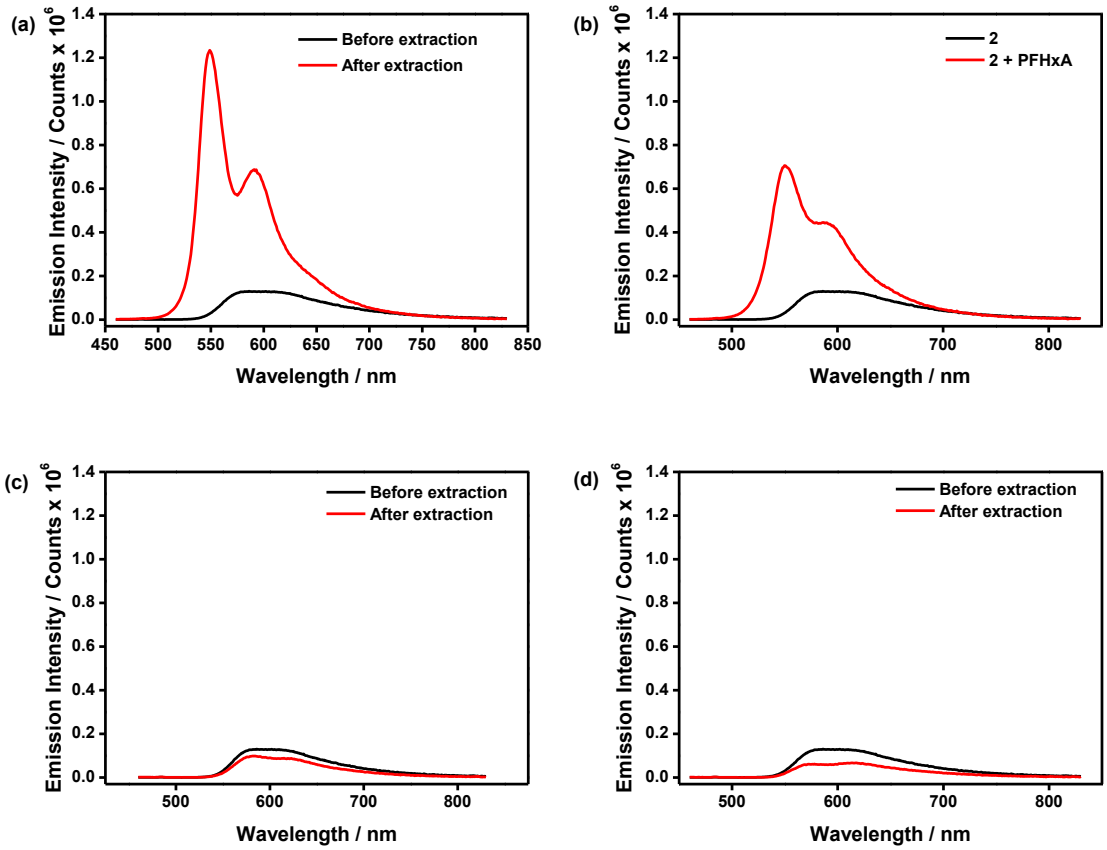

Figure S38 Emission spectra of **2** under different control experiments. (a) Emission spectra of **2** (6.23 μM) in 70% *n*-hexane-$CHCl_3$ (2 mL) before and after extraction with PFHxA (84 mM) in deionized water (2 mL). (b) Emission spectra of a mixture of **2** (6.23 μM) and PFHxA (84 mM) in 2 mL of 70% *n*-hexane-$CHCl_3$. (c) Emission spectra of **2** (6.23 μM) in 70% *n*-hexane-$CHCl_3$ (2 mL) before and after extraction with $C_6F_{13}COONa$ (84 mM) in deionized water (2 mL). (d) Emission spectra of **2** (6.23 μM) in 70% *n*-hexane-$CHCl_3$ (2 mL) before and after extraction with 0.2 M HNO_3 (2 mL).

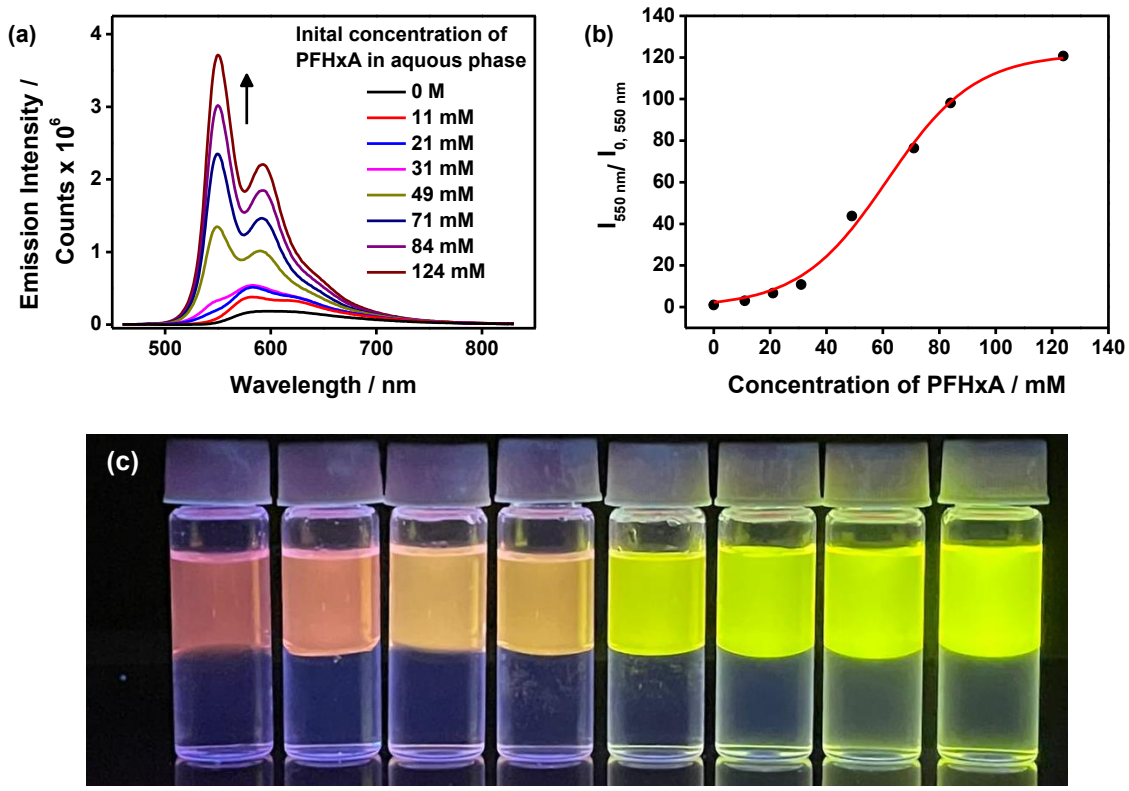

Figure S39 (a) Emission spectra of **2** (6.23 μM) in 70% *n*-hexane-$CHCl_3$ (2 mL) after extraction with different concentrations of PFHxA in deionized water (2 mL). The excitation wavelength is 425 nm. (b) Plot of relative emission intensity at 550 nm of the organic phase against concentration of PFHxA in deionized water. (c) A photograph showing **2** (6.23 μM) in 70% *n*-hexane-$CHCl_3$ (2 mL) after extraction with different concentrations of PFHxA in deionized water . The concentration of PFHxA in the aqueous phase from left to right is: 0 M, 11 mM, 21 mM, 31 mM, 49 mM, 71 mM, 84 mM, 124 mM. The photos were taken using a smartphone with a 450 nm filter and a UV light source (λ_{ex} = 365 nm).

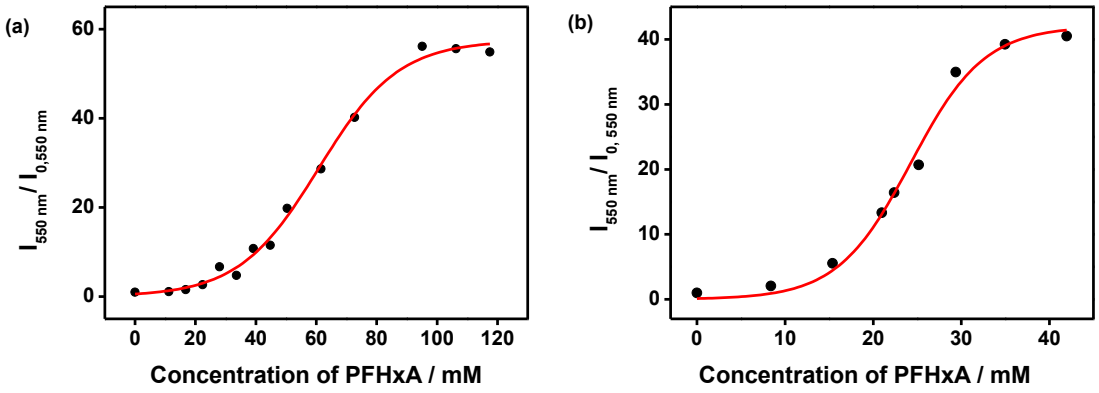

Figure S40 Plots of relative emission intensity at 550 nm of **2** (1.25 μM) in 70% *n*-hexane-$CHCl_3$ (2 mL) against concentration of PFHxA in 2 mL (a) deionized water and (b) 2 M NaCl.

References

(1) Miyaura, N.; Suzuki, A. Palladium-catalyzed Reaction of 1-Alkenylboronates with Vinylic Halides: (1Z,3E)-1-Phenyl-1,3-octadiene. In *Organic Syntheses*, **2003**; pp 130–130.
(2) Coulson, D. R.; Satek, L. C.; Grim, S. O. Tetrakis(triphenylphosphine)palladium(0). In *Inorganic Syntheses*, Inorganic Syntheses, **1972**; pp 121–124.
(3) Van Thong, P.; Thom, D. T.; Chi, N. T. T. Synthesis and Structure of Two Platinum(II) Complexes Bearing N-heterocyclic Carbene and Dimethyl Sulfoxide. *Vietnam J. Chem.* 2018, ***56***, 146–151.
(4) Ávila, E. P.; de Oliveira, L. A.; Neto, B. A. D.; de Almeida, M. V.; Pliego Jr, J. R. Flavanone-enabled CuAAC Reaction: Noninnocent Reagents Driving a Mononuclear Mechanism Over the Dinuclear Paradigm. *Chem. Eur. J.* 2025, ***31***, e202500121.
(5) Mello, J. V.; Finney, N. S. Convenient Synthesis and Transformation of 2,6-Dichloro-4-iodopyridine. *Org. Lett.* 2001, ***3***, 4263–4265.
(6) Li, Y.; Huffman, J. C.; Flood, A. H. Can Terdentate 2,6-Bis(1,2,3-triazol-4-yl)Pyridines Form Stable Coordination Compounds? *Chem. Commun.* 2007, 2692–2694.
(7) Schulze, B.; Winter, A.; Friebe, C.; Birckner, E.; Schubert, U. S. Soluble Pt^{II}-Containing Polymers Based on a 2,6-Bis(1*H*-1,2,3-triazol-4-yl)-4-ethynylpyridine Ligand. *ACS Macro Lett.* 2017, ***6***, 181–184.
(8) *Gaussian 16, Revision C.01,*; Frisch, M. J.; Trucks, G. W.; Schlegel, H. B.; Scuseria, G. E.; Robb, M. A.; Cheeseman, J. R.; Scalmani, G.; Barone, V.; Petersson, G. A.; Nakatsuji, H.; Li, X.; Caricato, M.; Marenich, A. V.; Bloino, J.; Janesko, B. G.; Gomperts, R.; Mennucci, B.; Hratchian, H. P.; Ortiz, J. V.; Izmaylov, A. F.; Sonnenberg, J. L.; Williams-Young, D.; Ding, F.; Lipparini, F.; Egidi, F.; Goings, J.; Peng, B.; Petrone, A.; Henderson, T.; Ranasinghe, D.; Zakrzewski, V. G.; Gao, J.; Rega, N.; Zheng, G.; Liang, W.; Hada, M.; Ehara, M.; Toyota, K.; Fukuda, R.; Hasegawa, J.; Ishida, M.; Nakajima, T.; Honda, Y.; Kitao, O.; Nakai, H.; Vreven, T.; Throssell, K.; Montgomery, J. A., Jr.; Peralta, J. E.; Ogliaro, F.; Bearpark, M. J.; Heyd, J. J.; Brothers, E. N.; Kudin, K. N.; Staroverov, V. N.; Keith, T. A.; Kobayashi, R.; Normand, J.; Raghavachari, K.; Rendell, A. P.; Burant, J. C.; Iyengar, S. S.; Tomasi, J.; Cossi, M.; Millam, J. M.; Klene, M.; Adamo, C.; Cammi, R.; Ochterski, J. W.; Martin, R. L.; Morokuma, K.; Farkas, O.; Foresman, J. B.; Fox, D. J. Gaussian, Inc., Wallingford CT: 2016.
(9) Perdew, J. P.; Burke, K.; Ernzerhof, M. Generalized Gradient Approximation Made Simple. *Phys. Rev. Lett.* 1996, ***77***, 3865–3868.
(10) Andrae, D.; Häußermann, U.; Dolg, M.; Stoll, H.; Preuß, H. Energy-Adjusted Ab Initio Pseudopotentials for the Second and Third Row Transition Elements. *Theor. Chim. Acta* 1990, ***77***, 123–141.
(11) Barone, V.; Cossi, M. Quantum Calculation of Molecular Energies and Energy Gradients in Solution by a Conductor Solvent Model. *J. Phys. Chem. A* 1998, ***102***, 1995–2001.
(12) Wang, J.; Cieplak, P.; Kollman, P. A. How Well Does a Restrained Electrostatic Potential (RESP) Model Perform in Calculating Conformational Energies of Organic and Biological molecules? *J. Comput. Chem.* 2000, ***21***, 1049–1074.
(13) Lu, T.; Chen, F. Multiwfn: A Multifunctional Wavefunction Analyzer. *J. Comput. Chem.* 2012, ***33***, 580–592.

(14) Wang, J.; Wolf, R. M.; Caldwell, J. W.; Kollman, P. A.; Case, D. A. Development and Testing of a General Amber Force Field. *J. Comput. Chem.* 2004, ***25***, 1157–1174.
(15) Allen, A. E. A.; Payne, M. C.; Cole, D. J. Harmonic Force Constants for Molecular Mechanics Force Fields via Hessian Matrix Projection. *JCTC* 2018, ***14***, 274–281.
(16) Zheng, X.; Chan, M. H.-Y.; Chan, A. K.-W.; Cao, S.; Ng, M.; Sheong, F. K.; Li, C.; Goonetilleke, E. C.; Lam, W. W. Y.; Lau, T.-C.; et al. Elucidation of the Key Role of Pt···Pt Interactions in the Directional Self-assembly of Platinum(II) Complexes. *Proc. Natl. Acad. Sci. U.* 2022, ***119***, e2116543119.
(17) Chan, T. H.-Y.; Chen, Z.; Leung, M.-Y.; Chan, M. H.-Y.; Wong, E. K.-H.; Tang, W. K.; Yam, V. W.-W. Thermoresponsive Platinum(II) 2,6-Di(pyrid-2-yl)pyrazine Complexes with Unusual Aggregation Behavior upon Heating. *J. Am. Chem. Soc.* 2025, ***147***, 24941–24949.
(18) Sobtop, Version 1.0 (dev5). http://sobereva.com/soft/Sobtop (accessed November, 2025).
(19) Van Der Spoel, D.; Lindahl, E.; Hess, B.; Groenhof, G.; Mark, A. E.; Berendsen, H. J. C. GROMACS: Fast, Flexible, and Free. *J. Comput. Chem.* 2005, ***26***, 1701–1718.